force vertical to the plate, and the cells were cultured for 1 d, allowing the formation of an NHDF sheet containing HUVECs.

1.6 Construction of vascularized NHDF sheets by seeding HUVECs onto NHDF sheets

Using the Mag-TE method described above, NHDF sheets without HUVECs were constructed. Subsequently, HUVECs (5×10^4 cells) or NHEKs (1.5×10^5 cells, control) were seeded onto NHDF sheets. Sheets were cultured in HuMedia-EG2 for 5 d in order to induce angiogenesis by HUVECs.

Fluorescence microscopy was performed using CellTracker™ (Molecular Probes); HUVECs and NHEKs were pre-stained with CMFDA (5-chloromethylfluoroscein diacetate; Molecular Probes), fluorescent-stained cells were seeded onto NHDF sheets and the formation of capillaries was periodically observed by fluorescence microscopy (Olympus Corp.). A time-course analysis of HUVEC areas was performed by the computerized image analysis of the number of pixels occupied by HUVEC-containing tubule areas ($n = 4$). Briefly, the image analysis of fluorescence images (image size, 1.21×10^6 pixels) was carried out using an image analysis program (Adobe Photoshop 6.0, Adobe Systems Inc.). Fluorescent areas (tubule areas) in the images were selected by magic wand tool, and the number of pixels occupied by tubule area was obtained.

1.7 Histology

For histological evaluation, cell sheets were washed with PBS, fixed in 10% formalin solution and embedded in paraffin. Thin (4 μm) slices were placed on silanized slides for immunohistochemistry or staining with hematoxylin-eosin (H&E). For immunohistochemistry, the primary antibodies used were rabbit anti-rat type I collagen (LSL), rabbit anti-human fibronectin (DakoCytomation), or anti-rabbit von Willebrand factor (vWF; DakoCytomation). Biotinylated goat anti-rabbit immunoglobulin (DakoCytomation) was used as a secondary antibody. Briefly, sections were incubated with 1% bovine serum albumin at 37°C for 30 min in order to block background staining, followed by incubation at 37°C for 60 min each with primary and secondary antibodies. Thereafter, slices were incubated at 37°C for 30 min with peroxidase-conjugated streptavidin (DakoCytomation). Each step was followed by washing with PBS. Peroxidase activity was visualized after soaking at room temperature for 10 min in 0.02% diaminobenzidine tetrahydrochloride containing 0.005% hydrogen peroxide (brown staining indicates peroxidase activity). Slides were also double-stained with Berlin blue (Ito *et al.*, 2004c) (blue staining indicates magnetite in MCLs). In negative control sections, primary antibodies were replaced with an unrelated monoclonal antibody.

For transmission electron microscopy, culture media were removed from the wells and were substituted with phosphate-buffered washing solution. Subsequent to all pre-embedding procedures, specimens were dehydrated in an ascending alcohol series. Fixed cells were then transferred and incubated in a propylene–epon mixture. From the embedded specimens, 1-μm serial sections were cut with an ultra-microtome (Ivan Sorvall) and were observed under a transmission electron microscope (H7000, Hitachi High-Technologies Corp.).

2. Results and Discussion

2.1 Magnetite nanoparticle uptake by cells and its effect on proliferation

The growth of NHDFs or HUVECs in medium containing MCLs (net magnetite concentration, 100 pg/cell) was compared with the growth in a medium without MCLs in order to investigate MCL toxicity against NHDFs or HUVECs. As shown in **Figure 1(a)**, MCLs did not inhibit the growth of NHDFs or HUVECs at the concentration studied.

As shown in Figure 1(**b**), the amounts of magnetite nanoparticles taken up by NHDFs and HUVECs differed; 24 h after the addition of MCLs, HUVECs took up 34 pg of magnetite per cell, whereas NHDFs took up 14 pg of magnetite per cell. Consequently, both cell types were sufficiently labeled magnetically to be attracted by a magnet (magnetic induction, 0.40 T). We reported previously that canine urothelial cells that took up 8 pg of magnetite per cell formed a sheet-like construct using the magnet (Ito *et al.*, 2005b). Therefore, we think that the NHDF sheet can be formed by Mag-TE. In subsequent experiments, MCLs were added to NHDFs or HUVECs at a concentration of 100 pg/cell, followed by a 24-h incubation period.

For clinical applications, MCL toxicity is an important issue. We previously reported that MCLs do not adversely affect proliferation of several types of normal cells within the range of MCL concentrations tested (i.e., human aortic endothelial cells [HAECs], <100 pg-magnetite/cell (Ito *et al.*, 2004c); human keratinocytes, <50 pg/cell (Ito *et al.*, 2004a); human smooth muscle cells, <100 pg-magnetite/cell (Ito *et al.*, 2005b); human mesenchymal stem cells [MSCs], <100 pg/cell (Ito *et al.*, 2004b)), and we observed no effects on MSC differentiation (Ito *et al.*, 2004b). However, further study is needed in order to assess the toxicity of residual magnetic nanopartilces in the grafts before Mag-TE can be used clinically.

2.2 Construction of NHDF sheets by Mag-TE

Magnetically labeled NHDFs were seeded onto 24-well ultralow-attachment plates and a 30-mm neodymium magnet was then placed under the plate. Because the magnetic density (0.40 T) was essentially even throughout the culture areas of the 24-well

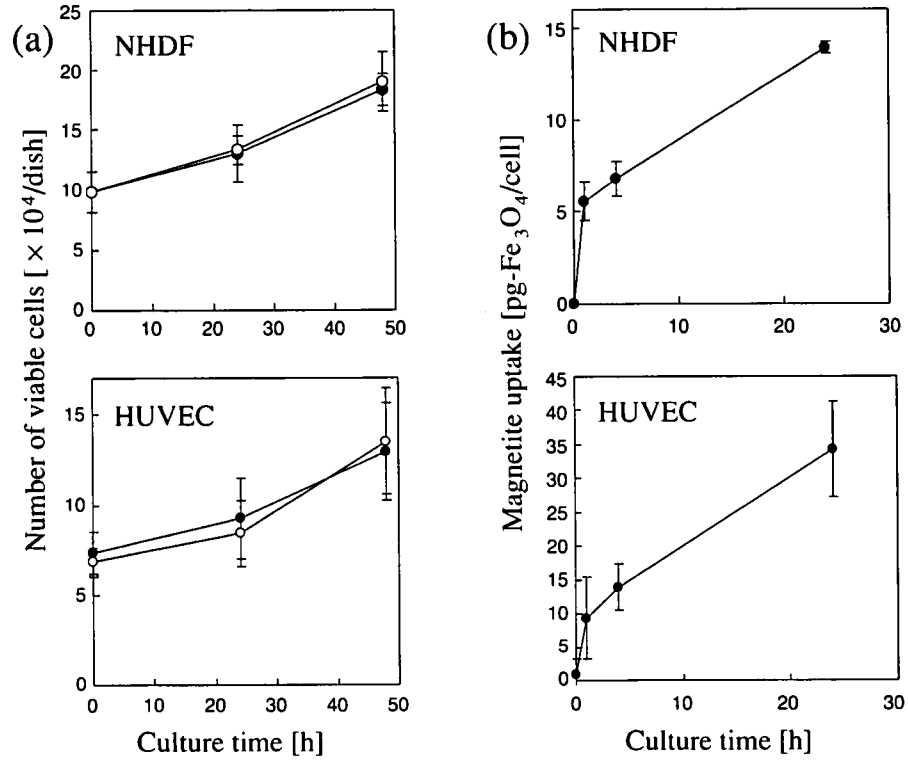

Fig. 1 MCL uptake and cell proliferation. MCL toxicity was examined by assessing cell growth after addition of MCLs (a). Open circles, no addition of MCLs; closed circles, addition of MCLs at 100 pg/cell. Magnetite nanoparticle uptake after addition of MCLs (100 pg/cell) was measured using the potassium thiocyanate method (b). Data points are means ± SD of duplicates

ultralow-attachment plates (Ito *et al.*, 2004a), NHDFs were rapidly attracted to the magnet and accumulated evenly over the bottom of the plate. After a 24-h incubation period, NHDF sediments shrank slightly and formed a sheet-like structure. In contrast, NHDFs without MCLs or with MCLs in the absence of a magnet did not form evenly contiguous cell sheets nor did they attach to the ultralow-attachment plates, but rather formed small spheroids (data not shown). **Figure 2(a)** shows an NHDF sheet constructed by Mag-TE; the sheets had a black-brown color, which is the color of magnetite. NHDF sheets constructed by Mag-TE shrank slightly (the decrease in the diameter was 20%) at 24 h after culture in the presence of a magnet. When the magnet was removed from the bottom of the plates, the sheets were detached from the bottom of the 24-well ultralow-attachment plates, and could be harvested without enzymatic digestion.

It has been observed and documented in 2D and 3D angiogenesis models using HUVEC that ECM components (type I collagen (Korff and Augustin, 1999), fibrin (Vailhe *et al.*, 1996), or matrigel (Kubota *et al.*, 1988)) promote capillary-like structure formation. Thus, ECM deposition is essential for constructing vascularized 3D tissues, particularly in scaffold-less cell sheets. It is generally difficult to fabricate 3D tissue constructs without using 3D scaffolds, due to the lack of cell adherence via cell–cell junctions, particularly in the vertical direction. This non-adherence may be caused by enzymatic digestion of ECM. To overcome this difficulty, Yamato *et al.* (2001) used a thermo-responsive culture surface grafted to poly (*N*-isopropylacrylamide) (PIPAAm), and recovered monolayer cell sheets grown on ECM deposited on the culture surface; because digestive enzymes were not used, the ECM remained intact and enhanced cell–cell attachment. Thus, this method of "cell sheet engineering" may be a viable alternative approach to tissue engineering. We developed a novel methodology, termed "Mag-TE", for the fabrication of cell sheets. We used magnetic attraction as a physical approach for enhancing layered cell–cell interactions.

We investigated whether ECM components were produced during NHDF sheet formation by Mag-TE. Cross-sectional observation by H&E staining revealed that NHDFs formed cell sheets of approximately 200 μm in thickness (Figure 2(b)) and containing Berlin blue-positive magnetite nanoparticles within the sheet (Figure 2(c)). Immunohistochemical staining revealed that ECM components such as fibronectin (Figure 2(d)) and type I collagen (Figure 2(e)), which are known to be major dermal ECM components and are known to promote capillary formation (Vailhe *et al.*, 2001), were deposited within the constructed NHDF sheets. Cell-ECM

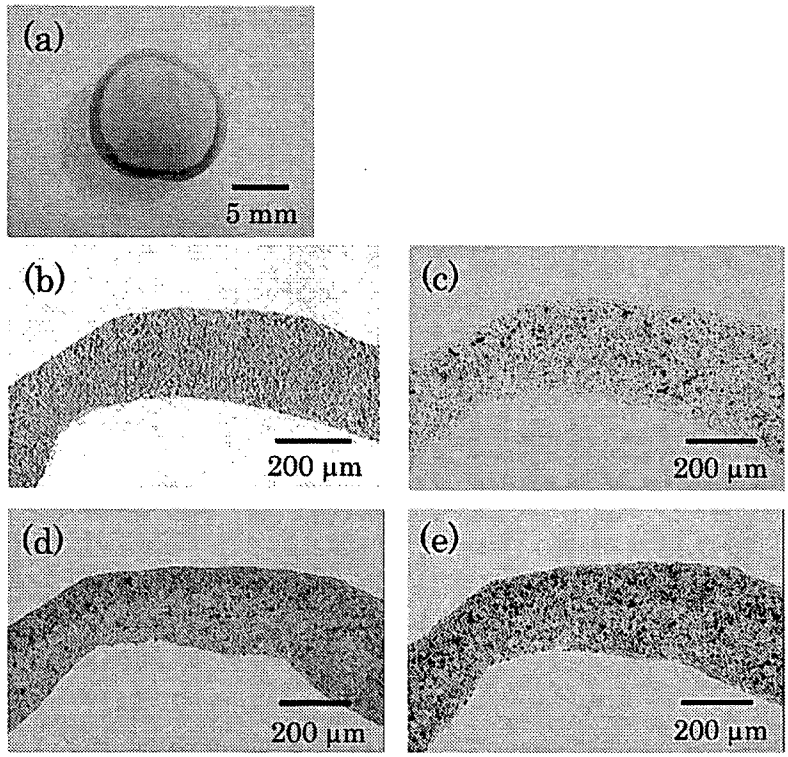

Fig. 2 Histological examination of fabricated NHDF sheets: (a) Bright-field micrograph of NHDF sheet constructed by Mag-TE; (b) Bright-field micrograph of hematoxylin/eosin-stained cross-sections of NHDF sheets constructed by Mag-TE; (c) Negative control using unrelated monoclonal antibody double-stained with Berlin blue (blue). Immunohistochemical stains for fibronection (brown, (d)) or type I collagen (brown, e) double-stained with Berlin blue (blue)

interactions can generate mechanical forces that can alter the structure of the surrounding ECM, which has been most convincingly shown in the case of fibroblast and $\alpha 2\beta 1$ integrin-mediated collagen gel contraction (Schiro *et al.*, 1991). These results suggest that collagen contraction due to NHDF-ECM interactions is involved in sheet shrinkage. The mechanism of ECM deposition remains to be elucidated, but we believe that the very close cell–cell interactions under 3D co-culture with magnetic force can elicit ECM deposition. ECM components deposited by cells within cell sheets during 3D-culture remain intact because the Mag-TE technique allows cell sheets to be harvested from the culture surface without enzymatic treatment. This point may play an important role in post-transplantation.

Fibroblasts are an integral component of all tissues; they contribute to architecture by producing ECM that serves as scaffolding for various organ structures, including vasculature. In addition, fibroblasts are a rich source of growth factors for self-stimulation and activation of other cell types in the microenvironment. In the present study, NHDF was selected as a model for construction of vascularized tissue, and two methods were employed in order to form capillaries *in* or *on* NHDF sheets.

2.3 Formation of capillaries in NHDF sheets

In order to produce capillaries within NHDF sheets, magnetically labeled NHDFs and HUVECs were admixed and seeded into ultralow-attachment plate. When the cells were co-cultured in the presence of a magnet for 1 d, NHDF sheets incorporating HUVECs were formed (overall appearance was as shown in Figure 2(a)). **Figure 3** shows cross-sections of NHDF sheets incorporating HUVECs on day 1. HUVECs formed tube-like structures with lumens of 5–6 μm (Figure 3(a)), and some formed connected tube-like structures (Figure 3(b)) within the sheets. Transmission electron microscopy revealed that HUVECs within NHDF sheets formed vacuoles (Figure 3(c)), suggesting that 3D co-culture of HUVECs within NHDF sheets induced angiogenesis.

2.4 Formation of capillaries on NHDF sheets

Alternatively, in order to construct capillaries on NHDF sheets, HUVECs were seeded onto NHDF sheets constructed by Mag-TE. **Figures 4(a)–(d)** show fluorescence microscopic images of HUVECs on NHDF sheets. HUVECs adhered to the NHDF sheets at 4 h after seeding (Figure 4(a)); extended on day 1 (Figure 4(b)); elongated and connected between cells on day 2 (Figure 4(c)); and finally organized into network structures, which exhibited multiple branching

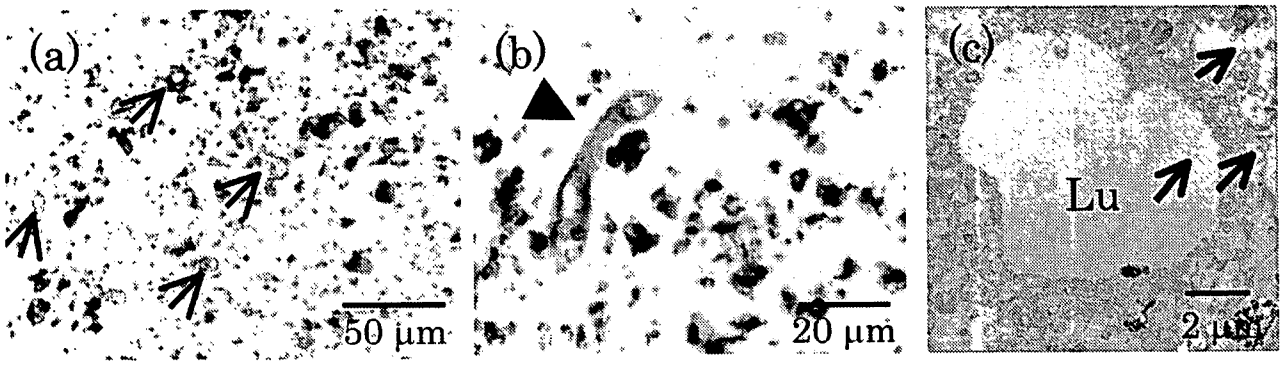

Fig. 3 Histological examination of HUVECs within NHDF sheets. Magnetically labeled NHDFs and HUVECs were admixed and seeded onto an ultralow-attachment plate, followed by placement of a magnet under the plate and coculture for 1 d. Bright-field micrographs of cross-sections of the cell sheets stained against vWF double-stained with tube-like structures and connection of two tube-like structures, respectively. (c) Transmission electron microscopy of cross-sections of fabricated cell sheets. Lumen (Lu) was evident. Arrows indicate magnetite particles

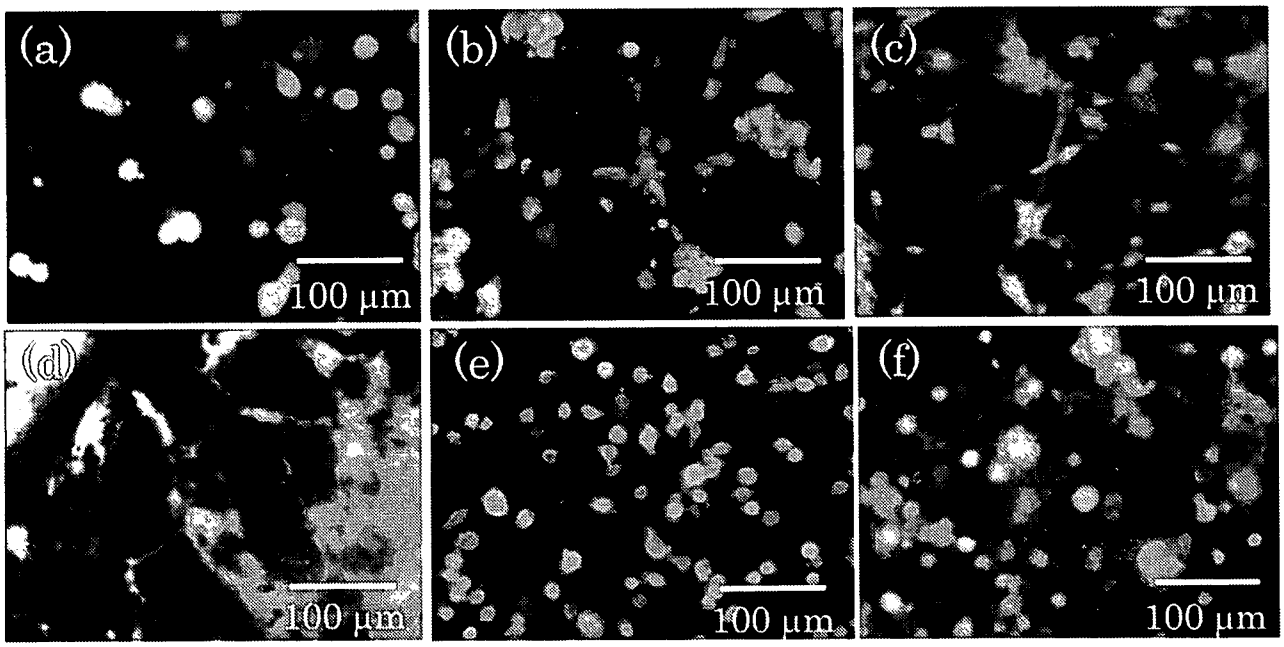

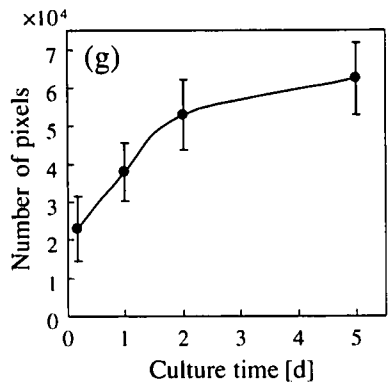

Fig. 4 Fluorescence images of HUVECs on NHDF sheets. Magnetically labeled NHDFs were seeded onto an ultralow-attachment plate, followed by placement of a magnet under the plate and culture for 1 d. Subsequently, HUVECs (a–d) or NHEKs (e and f) were seeded onto NHDF sheets. Cells were observed periodically by fluorescence microscopy. (a) and (e), 4 h; (b), 1 d; (c), 2 d; (d) and (f), 5 d. (g) Time-course analysis of HUVEC areas was performed by the computerized image analysis of the number of pixels occupied by HUVEC-containing tubule areas. Data points are means ± SD (n = 4)

points, on day 5 (Figure 4(d)). Time-course analysis of HUVEC areas was performed by computerized image analysis of the number of pixels occupied by HUVECs including tubule areas; the fluorescence area on the NHDF sheets increased (Figure 4(g)), thus suggesting that HUVECs proliferated and/or spread on the NHDF sheets for 5 d. On the other hand, although NHEKs adhered on the NHDF sheets at 4 h after

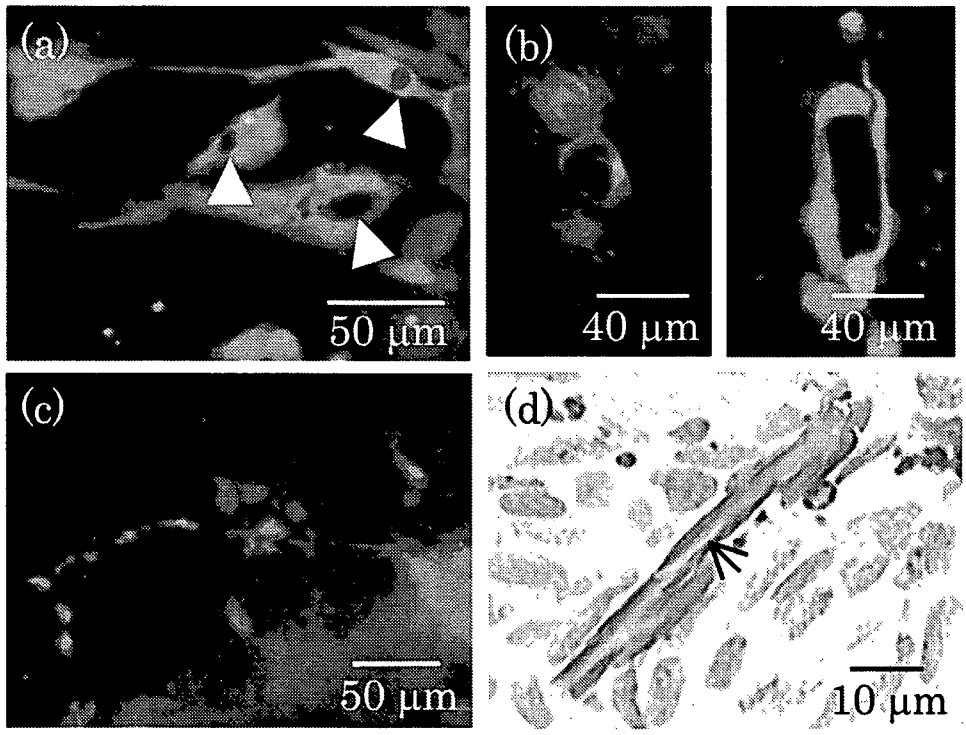

Fig. 5 Morphological changes of HUVECs on NHDF sheets. Fluorescence microscopy of HUVECs revealed vacuole (a, day 3, indicated by arrowheads) and lumen formation (b) consisting of two (left, day 5) or more cells (right, day 3), and sprouting of cord-like structures (c, day 5) on NHDF sheets. (d) Bright-field micrographs of immuno-staining against vWF (brown) double-stained with Berlin blue (blue) in thin slices (4 μm) of sheets revealed capillary lumen formation (indicated by an arrow) by HUVECs

co-culture (Figure 4(e)) and slightly increased in the cell number (data not shown), NHEKs did not organize cordlike network structures even after a 5-d culture period (Figure 4(f)).

Two major morphologic changes that regulate HUVEC tube development include lumen formation and sprouting, and these changes control how HUVECs interconnect into 3D networks. Fluorescence microscopic images of HUVECs co-cultured on NHDF sheets revealed vacuoles (**Figure 5(a)**) and lumens consisting of two or three HUVECs (Figure 5(**b**)), as well as sprouting with long cord-like structures (>250 μm, Figure 5(c)). Immuno-staining against vWF on thin slices (4 μm) of the sheets revealed capillary lumen formation surrounded by HUVECs (Figure 5(**d**)).

Tube-like formations of HUVECs were observed in both cases (Figures 3–5) after short-term 3D co-culture, but there may be differences between two methods with regard to the angiogenesis process. HUVECs incorporated within the NHDF sheets formed tube-like structures on day 1 (Figure 3), but the cross-sectional analysis revealed that the number of vWF-positive tube-like structures did not increase until at least 5 d after co-culture (data not shown). On the other hand, when HUVECs were seeded onto NHDF sheets, HUVECs proliferated and/or spread during the 5-d incubation period (Figure 4(g)). We suppose that the poor growth of HUVECs within the NHDF sheet was mainly caused by contact inhibition, i.e., HUVECs could not spread in the highly dense NHDF sheets.

In the present study, we showed that NHDF sheets constructed by Mag-TE induced HUVECs to generate a primitive cord-like network (Figure 4(d)), via vacuole (Figure 5(a)) and lumen formation (Figure 5(b)), and sprouting (Figure 5(c)), which mimic the processes observed during early angiogenesis *in vivo*. For application to tissue engineering, transplantation of preformed capillary structures may be crucial for graft survival. HUVEC-derived cords formed in 3D collagen gels have been shown to survive and inosculate with mouse microvessels after transplantation (Schechner *et al.*, 2000). Because blood vessels are stabilized by association with pericytes, including embryonic fibroblasts (Levenberg *et al.*, 2005) or smooth muscle cells, co-culture of these cells may be a possible approach. Previously, we succeeded in constructing Mag-tissue engineered small-diameter vascular tissue consisting of heterotypic layers of endothelial cells, smooth muscle cells and fibroblasts (Ito *et al.*, 2005b). Thus, the Mag-TE technique can be applied to construct a vascularized NHDF sheets incorporating pericytes or smooth muscle cells for vascular stabilization after transplantation. Furthermore, Mag-TE technique can be used for micro-patterning of

target cells, including HUVECs (unpublished results). Thus, we believe that designed capillaries can be formed on NHDF sheets by using micro-patterned magnets, and we are planning to construct native-like thick 3D structures consisting of multi-layer of the sheet.

Conclusions

We developed a novel methodology to construct vascularized cell sheets using MCLs and magnetic force ("Mag-TE"). Mag-TE allowed the *in vitro* fabrication and harvesting of NHDF sheets containing ECM and capillaries, and this technique may be applied to the engineering of thick 3D tissues for nutrient or oxygen supply.

Acknowledgment

This work was supported in part by the 21st Century COE Program 'Nature-Guided Materials Processing' and by a Grant-in-Aid for Scientific Research (No. 17760622) and by a Grant-in-Aid for Scientific Research on Priority Areas (No. 17066003) from the Ministry of Education, Sports, Science and Technology, Japan.

Literature Cited

Ito, A., M. Hayashida, H. Honda, K. Hata, H. Kagami, M. Ueda and T. Kobayashi; "Construction and Harvest of Multilayered Keratinocyte Sheets Using Magnetite Nanoparticles and Magnetic Force," *Tissue Eng.*, **10**, 873–880 (2004a)

Ito, A., E. Hibino, H. Honda, K. Hata, H. Kagami, M. Ueda and Kobayashi; "A New Methodology of Mesenchymal Stem Cell Expansion Using Magnetic Nanoparticles," *Biochem. Eng. J.*, **20**, 119–125 (2004b)

Ito, A., Y. Takizawa, H. Honda, K. Hata, H. Kagami, M. Ueda and T. Kobayashi; "Tissue Engineering Using Magnetite Nanoparticles and Magnetic Force: Heterotypic Layers of Cocultured Hepatocytes and Endothelial Cells," *Tissue Eng.*, **10**, 833–840 (2004c)

Ito, A., K. Ino, T. Kobayashi and H. Honda; "The Effect of RGD Peputide-Conjugated Magnetite Cationic Liposomes on Cell Growth and Cell Sheet Harvesting," *Biomaterials*, **26**, 6185–6193 (2005a)

Ito, A., K. Ino, M. Hayashida, T. Kobayashi, H. Matsunuma, H. Kagami, M. Ueda and H. Honda; "Novel Methodology for Fabrication of Tissue-Engineered Tubular Constructs Using Magnetite Nanoparticles and Magnetic Force," *Tissue Eng.*, **11**, 1553–1561 (2005b)

Ito, A., E. Hibino, C. Kobayashi, H. Terasaki, H. Kagami, M. Ueda, T. Kobayashi and H. Honda; "Construction and Delivery of Tissue-Engineered Human Retinal Pigment Epithelial Cell Sheets Using Magnetite Nanoparticles and Magnetic Force," *Tissue Eng.*, **11**, 489–496 (2005c)

Korff, T. and H. G. Augustin; "Tensional Forces in Fibrillar Extracellular Matrices Control Directional Capillary Sprouting," *J. Cell Sci.*, **112**, 3249–3258 (1999)

Kubota, Y., H. K. Kleinman, G. R. Martin and T. J. Lawley; "Role of Laminin and Basement Membrane in the Morphological Differentiation of Human Endothelial Cells into Capillary-Like Structures," *J. Cell Biol.*, **107**, 1589–1598 (1988)

Langer, R. and J. P. Vacanti; "Tissue Engineering," *Science*, **260**, 920–926 (1993)

Levenberg, S., J. Rouwkema, M. Macdonald, E. S. Garfein, D. S. Kohane, D. C. Darland, R. Marini, C. A. van Blitterswijk, R. C. Mulligan, P. A. D'Amore and R. Langer; "Engineering Vascularized Skeletal Muscle Tissue," *Nat. Biotechnol.*, **23**, 879–884 (2005)

Lewin, M., N. Carlesso, C. H. Tung, X. W. Tang, D. Cory, D. T. Scadden and R. Weissleder; "Tat Peptide-Derivatized Magnetic Nanoparticles Allow *in vivo* Tracking and Recovery of Progenitor Cells," *Nat. Biotechnol.*, **18**, 410–414 (2000)

Lorimier, S., P. Gillery, W. Hornebeck, F. Chastang, D. Laurent-Maquin, S. Bouthors, C. Droulle, G. Potron and F. X. Maquart; "Tissue Origin and Extracellular Matrix Control Neutral Proteinase Activity in Human Fibroblast Three-Dimensional Cultures," *J. Cell Physiol.*, **168**, 188–198 (1996)

Miltenyi, S., W. Muller, W. Weichel and A. Radbruch; "High Gradient Magnetic Cell Separation with MACS," *Cytometry*, **11**, 231–238 (1990)

Moore, L. R., M. Zborowski, L. Sun and J. J. Chalmers; "Lymphocyte Fractionation Using Immunomagnetic Colloid and a Dipole Magnet Flow Cell Sorter," *J. Biochem. Biophys. Methods*, **37**, 11–33 (1998)

Owen, C. S. and N. L. Sykes; "Magnetic Labeling and Cell Sorting," *J. Immunol. Methods*, **73**, 41–48 (1984)

Radbruch, A., B. Mechtold, A. Thiel, S. Miltenyi and E. Pfluger; "High-Gradient Magnetic Cell Sorting," *Methods Cell Biol.*, **42**, 387–403 (1994)

Schaffer, C. J. and L. B. Nanney; "Cell Biology of Wound Healing," *Int. Rev. Cytol.*, **169**, 151–181 (1996)

Schechner, J. S., A. K. Nath, L. Zheng, M. S. Kluger, C. C. Hughes, M. R. Sierra-Honigmann, M. I. Lorber, G. Tellides, M. Kashgarian, A. L. Bothwell and J. S. Pober; "*In vivo* Formation of Complex Microvessels Lined by Human Endothelial Cells in an Immunodeficient Mouse," *Proc. Natl. Acad. Sci., USA*, **97**, 9191–9196 (2000)

Schiro, J. A., B. M. Chan, W. T. Roswit, P. D. Kassner, A. P. Pentland, M. E. Hemler, A. Z. Eisen and T. S. Kupper; "Integrin Alpha 2 Beta 1 (VLA-2) Mediates Reorganization and Contraction of Collagen Matrices by Human Cells," *Cell*, **67**, 403–410 (1991)

Sengar, R. D.; "Molecular Framework for Angiogenesis: a Complex Web of Interactions between Extravasated Plasma Proteins and Endothelial Cell Proteins Induced by Angiogenesis Cytokines," *Am. J. Path.*, **149**, 1–7 (1996)

Sephel, G. C., R. Kennedy and S. Kudravi; "Expression of Capillary Basement Membrane Components during Sequential Phases of Wound Angiogenesis," *Matrix Biol.*, **15**, 263–279 (1996)

Shimizu, K., A. Ito and H. Honda; "Enhanced Cell-Seeding into 3D Porous Scaffolds by Use Magnetite Nanoparticles," *J. Biomed. Mater. Res. B. Appl. Biomater.*, **77**, 265–272 (2005)

Shinkai, M. and A. Ito; "Functional Magnetic Particles for Medical Application," *Adv. Biochem. Eng. Biotechnol.*, **91**, 191–220 (2004)

Shinkai, M., M. Yanase, H. Honda, T. Wakabayashi, J. Yoshida and T. Kobayashi; "Intracellular Hyperthermia for Cancer Using Magnetite Cationic Liposomes: *in vitro* Study," *Jpn. J. Cancer Res.*, **87**, 1179–1183 (1996)

Vailhe, B., X. Ronot, M. Lecomte, N. Wiernsperger and L. Tranqui; "Description of an *in vitro* Angiogenesis Model Designed to Test Antiangiogenic Molecules," *Cell Biol. Toxicol.*, **12**, 341–344 (1996)

Vailhe, B., D. Vittet and J. J. Feige; "*In vitro* Models of Vasculogenesis and Angiogenesis," *Lab. Invest.*, **81**, 439–452 (2001)

Weckoth, M., A. Vaheri, J. Lauharanta, T. Sorsa and Y. T. Konttinen; "Matrix Metalloproteinases, Gelatinase and Collagenase, in Chronic Leg Ulcers," *J. Invest. Dermatol.*, **106**, 1119–1124 (1996)

Yamato, M., M. Utsumi, A. Kushida, C. Konno, A. Kikuchi and T. Okano; "Thermo-Responsive Culture Dishes Allow the Intact Harvest of Multilayered Keratinocyte Sheets without Dispase by Reducing Temperature," *Tissue Eng.*, **7**, 473–480 (2001)

THE JOURNAL OF BIOLOGICAL CHEMISTRY VOL. 282, NO. 6, pp. 4152–4161, February 9, 2007

Chondroitin Sulfate *N*-Acetylgalactosaminyltransferase-1 Plays a Critical Role in Chondroitin Sulfate Synthesis in Cartilage*[S]

Received for publication, July 19, 2006, and in revised form, October 23, 2006 Published, JBC Papers in Press, December 4, 2006, DOI 10.1074/jbc.M606870200

Kenichiro Sakai[‡§], Koji Kimata[‡], Takashi Sato[¶], Masanori Gotoh[¶], Hisashi Narimatsu[¶], Kenichi Shinomiya[§], and Hideto Watanabe[‡1]

From the [‡]Institute for Molecular Science of Medicine, Aichi Medical University, Nagakute, Aichi 480-1195, Japan, the [§]Department of Orthopedic Surgery, Tokyo Medical and Dental University, Bunkyo-ku, Tokyo 113-8519, Japan, and the [¶]Research Center for Glycoscience, National Institute of Advanced Industrial Science and Technology, Tsukuba, Ibaraki 305-8568, Japan

Cartilage destruction leads to severe joint diseases, such as osteoarthritis and spinal disorders with back pain, and cartilage regeneration is very inefficient. A major component of the cartilage extracellular matrix is the proteoglycan aggrecan that contains approximately 100 chondroitin sulfate (CS) chains, which impart water absorption and resistance to compression. Here, we demonstrate that chondroitin sulfate *N*-acetylgalactosaminyltransferase-1 (CSGalNAcT-1) plays a critical role in CS biosynthesis in cartilage. By *in situ* hybridization and real time reverse transcription-PCR of developing cartilage, CSGalNAcT-1 exhibited the highest level of expression. Its expression in chondrogenic ATDC5 cells correlated well with that of aggrecan core protein. In heterozygote and homozygote aggrecan-null cartilage where aggrecan transcription is decreased, CSGalNAcT-1 transcription diminished accordingly. Overexpression of the enzyme in chondrocytic cells further enhanced CS biosynthesis but not that of the aggrecan core protein, indicating that the enzyme activity is not saturated in the cells and that aggrecan synthesized in the overexpressing cells is heavier than the native molecule. Analysis of the CS chains synthesized in the overexpressing cells by gel chromatography and that of disaccharide composition revealed that the CS chains had similar length and sulfation patterns. Furthermore, adenoviral gene delivery of the enzyme into intervertebral discs displayed a substantial increase in the level of CS biosynthesis. These observations indicate that CSGalNAcT-1 overexpression increases the number of CS chains attached to aggrecan core protein. Our studies may lead to a new therapeutic intervention, ameliorating the outcome of cartilage degenerative diseases.

Cartilage is localized on joint surfaces and in the spine, where it forms the intervertebral discs and helps physical movement. The extracellular matrix of cartilage contains two major structural components: the fiber structure made of collagens and the proteoglycan aggregate. Whereas collagen fibers of types II, IX, and XI provide cartilage with tensile strength, the proteoglycan aggregate, composed of a large proteoglycan aggrecan, hyaluronan, and link protein, provides it with resistance to compression (1). Aggrecan consists of a core protein and approximately 100 chains of chondroitin sulfate (CS)[2] attached to the core protein (2, 3). Aggrecan is incorporated into the cartilage matrix by binding hyaluronan, and the CS chains impart water absorption. The CS content of aggrecan gradually diminishes with age, resulting in decreased water retention and aggravation of cartilage degeneration (4–6). This leads to severe joint diseases, such as osteoarthritis (7, 8) and spinal disorders with back pain (9, 10). Due to the lack of blood vessels and the presence of specific structural macromolecules, such as aggrecan, cartilage is one of the most difficult tissues to regenerate.

CS comprises repeating disaccharide units of GalNAc and glucuronic acid (GlcUA) residues with sulfate residues at various positions. CS biosynthesis (11) (Fig. 1*A*) is initiated by the transfer of a GalNAc residue to the linkage region of a GlcUA-β1,3-Gal-β1,3-Gal-β1,4-Xyl tetrasaccharide primer that is attached to a serine residue of the core protein. Then chain elongation occurs by the alternate addition of GalNAc and GlcUA residues. Enzyme activities that catalyze the initiation and elongation processes are termed glycosyltransferase-I and II activities, respectively (12). To date, six glycosyltransferases involved in CS synthesis have been identified (Fig. 1*B*): chondroitin sulfate synthase-1 (CSS-1)/chondroitin synthase (13), chondroitin sulfate synthase-2 (CSS-2)/chondroitin-polymerizing factor (14, 15), chondroitin sulfate synthase-3 (CSS-3) (16), chondroitin sulfate glucuronyltransferase (CSGlcAT) (17), and chondroitin sulfate *N*-acetylgalactosaminyltransferase-1 (18, 19) and -2 (20, 21) (CSGalNAcT-1 and -2, respectively). All of these enzymes have an N-terminal transmembrane domain and are localized to the Golgi apparatus, where CS biosyn-

* This work was supported by the New Energy and Industrial Technology Development Organization and by grants-in-aid for scientific research (C) (KAKENHI) (to H. W). The costs of publication of this article were defrayed in part by the payment of page charges. This article must therefore be hereby marked "*advertisement*" in accordance with 18 U.S.C. Section 1734 solely to indicate this fact.

[S] The on-line version of this article (available at http://www.jbc.org) contains supplemental Tables 1–3.

[1] To whom correspondence should be addressed: Institute for Molecular Science of Medicine, Aichi Medical University, Nagakute, Aichi 480-1195, Japan. Tel.: 81-561-62-3311 (ext. 2086); Fax: 81-561-63-3532; E-mail: wannabee@aichi-med-u.ac.jp.

[2] The abbreviations used are: CS, chondroitin sulfate; GlcUA, glucuronic acid; CSS-1, -2, and -3, chondroitin sulfate synthase-1, -2, and -3, respectively; CSGlcAT, chondroitin sulfate glucuronyltransferase; CSGalNAcT-1 and -2, chondroitin sulfate *N*-acetylgalactosaminyltransferase-1 and -2, respectively; GalNAcT, *N*-acetylgalactosaminyltransferase; GlcAT, glucuronyltransferase; cmd, cartilage matrix deficiency; RT, reverse transcription; HexA, hexuronic acid; E*n*, embryonic day *n*.

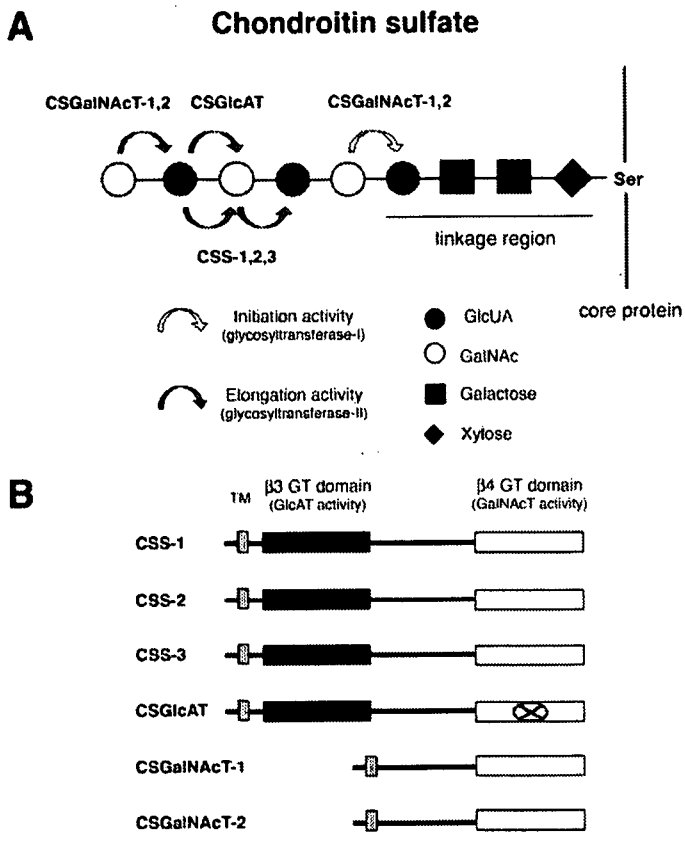

FIGURE 1. **CS biosynthesis and its related glycosyltransferases.** *A*, a schematic diagram of the catalytic activities of the glycosyltransferases involved in chondroitin sulfate synthesis. CS biosynthesis is initiated by the transfer of a GalNAc unit to the linkage region of a GlcUA-Gal-Gal-Xyl tetrasaccharide primer that is attached to a serine residue of the core protein. This is followed by chain elongation that occurs by the alternate addition of GalNAc and GlcUA residues. Six glycosyltransferases involved in CS synthesis have been identified. CSS-1, -2, and -3 exhibit both GalNAcT and GlcAT activities in chain elongation (glycosyltransferase-II activity). CSGlcAT exhibits only GlcAT-II activity. CSGalNAcT-1 and -2 exhibit GalNAcT activity in both the initiation and elongation processes (GalNAcT-I and -II activities). *B*, a schematic structural comparison of the six glycosyltransferases. Conserved domains in β1,3-galactosyltransferases or β1,4-galactosyltransferases are indicated as *closed* or *open boxes*. The putative transmembrane (*TM*) domains are indicated as *gray boxes*.

thesis takes place (22). CSS-1, CSS-2, CSS-3, and CSGlcAT form a family of glycosyltransferase enzymes. CSS-1, CSS-2, and CSS-3 contain two glycosyltransferase domains and exhibit both *N*-acetylgalactosaminyltransferase (GalNAcT) and glucuronyltransferase (GlcAT) activities in chain elongation. Thus, they have glycosyltransferase-II (both GalNAcT-II and GlcAT-II) activity. CSGlcAT has an inactive GalNAcT domain and exhibits only GlcAT-II activity. CSGalNAcT-1 and -2 have one glycosyltransferase domain and exhibit GalNAcT activity in both the initiation and elongation processes, indicating that CSGalNAcT-1 and -2 have both GalNAcT-I and -II activities. Thus, CS chain elongation may involve all six enzymes, whereas CS chain initiation probably involves only CSGalNAcT-1 and -2. Although individual enzymes have been biochemically characterized, the *in vivo* mechanism of CS biosynthesis is not fully understood. Since cartilage contains a large amount of CS, chondrocytes must be capable of efficiently synthesizing numerous CS chains. Elucidation of the mechanism of CS biosynthesis in cartilage would provide a basis for the development of a treatment promoting cartilage regeneration.

In this study, we identified CSGalNAcT-1 as the enzyme critical for cartilage CS biosynthesis. Overexpression of the enzyme in chondrocytic cells elevated the level of CS biosynthesis, and *in vivo* adenoviral gene delivery of the enzyme into the intervertebral disc resulted in a higher level of CS incorporation. The aggrecan synthesized in the CSGalNAcT-1-overexpressing cells had a higher number of CS chains. We term this molecule "superaggrecan" and propose a novel enzyme-based approach for the therapeutic intervention of cartilage degenerative diseases.

EXPERIMENTAL PROCEDURES

In Situ Hybridization—cDNA fragments encoding glycosyltransferases and aggrecan core protein were prepared by PCR using cDNA of differentiating ATDC5 cells and appropriate primers (supplemental Table 1). The PCR product was then subcloned into the pBluescript IISK(−) vector (Stratagene). RNA probes were prepared using cDNA prepared as described above and a DIG RNA labeling kit (Roche Applied Science). A humerus was obtained from an E16.5 mouse and fixed with 4% paraformaldehyde for 16 h at 4 °C. The samples were embedded in paraffin and sliced into 4-μm sections. *In situ* hybridization was performed as described previously (23).

Cell Culture—ATDC5 cells, a cell line established from chondrocytic cells of a mouse embryonal carcinoma, undergo all of the steps of chondrogenesis (24). The cells were cultured in a maintenance medium consisting of a 1:1 mixture of Dulbecco's modified Eagle's medium and Ham's F-12 medium containing 5% fetal bovine serum, 10 μg/ml human transferrin, 3×10^{-8} M sodium selenite, penicillin, and streptomycin. To induce chondrocyte differentiation, the cells at confluence were treated with 10 μg/ml of bovine insulin. N1511 cells, a cell line established from chondrocytic cells from the rib cage of a 4-week-old male p53-null mouse, undergo all of the steps of chondrogenesis (25). The cells were cultured in minimum essential medium α supplemented with 10% fetal bovine serum, penicillin, and streptomycin. Differentiation was similarly induced by combined treatment with of 1×10^{-6} M dexamethasone and 1×10^{-7} M rat parathorimone. LTC cells, a rat chondrosarcoma cell line, were cultured in Ham's F-12 medium containing 10% fetal bovine serum, penicillin, and streptomycin. 293A cells, an embryonic human kidney cell line, were cultured in Dulbecco's modified Eagle's medium containing 10% fetal bovine serum, 0.1 mM minimum essential medium nonessential amino acids, 2 mM L-glutamine, penicillin, and streptomycin. Cell culture was performed at 37 °C in a humidified atmosphere of 5% CO_2 in air. The medium was changed every other day.

Real Time RT-PCR—mRNA was isolated from ATDC5, N1511, and transfected LTC cells and cartilage of a cartilage matrix deficiency (cmd) mouse at E18.5 using Micro-Fast-Track™ (Invitrogen) according to the manufacturer's instructions. cDNA was synthesized using SuperScript™ First-Strand (Invitrogen) according to the manufacturer's instructions. The TaqMan probes contained a reporter dye at the 5′ end and a quencher dye at the 3′ end. To calculate the copy number, control vectors were prepared by PCR using appropriate primers and the cDNA obtained from N1511 cells, followed by subcloning of the fragment into pCRII-TOPO (Invitrogen). For CSS-3,

a BAC clone was used as the PCR template. Primers and probes used for real time RT-PCR are listed in supplemental Table 2. Primers for the control vector are listed in supplemental Table 3. Relative quantification of gene expression was performed using the Applied Biosystems ABI Prism 7700 sequence detection system (TaqMan). PCRs for all of the samples were performed in triplicate in 96-well optical plates using 5 ng of cDNA, 25 μl of TaqMan Universal PCR Mastermix (Applied Biosystems), 100 nM probe, 100 nM each primer, and water to a final volume of 50 μl. Thermocycling conditions comprised an initial holding step at 50 °C for 2 min, 95 °C for 10 min, and 50 cycles of 95 °C for 15 s and 60 °C for 60 s. To standardize mRNA levels, the primers for glyceraldehyde-3-phosphate dehydrogenase were used as internal controls.

Construction of Mammalian Expression Vectors of Glycosyltransferases and Establishment of Their Overexpressing Cell Lines—Full-length human cDNA encoding the glycosyltransferases was amplified by PCR using the Marathon Ready™ cDNA obtained from human bone marrow tissue (Clontech) as the template and two primers: 5′-AAGCTTCCCAAGCTTATGATGATGGTTCGCCGGGGGCT-3′ and 5′-TCTAGAGCTCTAGATCATGTTTTTTTGCTACTTGTCTTCTGT-3′ for CSGalNAcT-1; 5′-AAGCTTCCCAAGCTTGCGGGCATGGCCGCGCGCGG-3′ and 5′-TCTAGAGCTCTAGACATTAGGCTGTCCTCACTGA-3′ for CSS-1; 5′-AAGCTTCCCAAGCTTATGCGGGCATCGCTGCTGCTGT-3′ and 5′-TCTAGACGGGATCCTCAGGTGCTGTTGCCCTGCTCC-3′ for CSS-2; 5′-AAGCTTCCCAAGCTTACCACCATGCGACTGAGCTCCCT-3′ and 5′-TCTAGAGCTCTAGACTAAGTGCTATTGGCCTGCTCCT-3′ for CSGlcAT, which are attached with a HindIII or XbaI site (underlined), respectively. The amplified fragment was subcloned into pcDNA/Hygro (Invitrogen) using the HindIII and XbaI sites, as previously described (20). The CSGalNAcT-1/pcDNA3.1(+), CSS-1/pcDNA3.1(+), CSS-2/pcDNA3.1(+), and CSGlcAT/pcDNA3.1(+) vectors were constructed by subcloning the full-length cDNA into pcDNA3.1 (Invitrogen). LTC cells were transfected with these expression vectors (+) or pcDNA3.1(+) (as a mock control) using FuGENE6 (Roche Applied Science) according to the manufacturer's instructions. These cells were cultured in the presence of 750 μg/ml G418 (Nacalai) for 10 days. The expression levels of these enzymes were measured by real time RT-PCR. The stable cells overexpressing individual enzymes at similar levels were used.

Alcian Blue Staining—Cells were plated in 35-mm dishes. When the cells reached 80% confluence in a conditioned medium on day 2, they were washed in phosphate-buffered saline and fixed with 4% paraformaldehyde for 30 min. A humerus was obtained from an E16.5 mouse and fixed with 4% paraformaldehyde for 16 h at 4 °C. The samples were embedded in paraffin and sliced into 4-μm sections. Transduced vertebral sections were obtained as described below. The cells and deparaffinized sections were then stained using 0.1% Alcian blue in 0.1 M HCl at room temperature for 10 min.

Immunostaining—The transfected LTC cells were plated in 4-well culture slides. When the cells reached 30% confluence at day 2, they were washed in phosphate-buffered saline and fixed with 4% paraformaldehyde for 30 min. They were double-immunostained as previously described (25). For chondroitin 4-sulfate detection, mouse monoclonal anti-chondroitin 4-sulfate (LY111, ×200; Seikagaku) and Alexa Fluor™ 488-conjugated anti-mouse IgM (×1000) were used as the primary and secondary antibodies, respectively. For aggrecan core protein detection, rabbit polyclonal anti-aggrecan (×1000) (26) and Alexa Fluor™ 594-conjugated anti-rabbit IgG (×1000) were used as the primary and secondary antibodies, respectively. The specimen was observed using a Zeiss LSM 5 Pascal laser confocal microscope.

Characterization of Aggrecan—The transfected LTC cells were plated in a 100-mm culture dish. The cells and conditioned medium were collected separately at day 2 and extracted with 4 M guanidine hydrochloride, 50 mM Tris-HCl, pH 8.0, 10 mM EDTA, 1 mM phenylmethanesulfonyl fluoride, and 10 mM *N*-ethylmaleimide. The samples were stirred overnight at 4 °C and clarified by centrifugation in capped polycarbonate tubes (15,000 × *g*, 10 min, 4 °C). Portions of the samples were used for immuno-dot blot analysis. CsCl was added to obtain a density of 1.55 g/ml, and this was followed by ultracentrifugation under a dissociative condition in polyallomer tubes at 40,000 × *g* at 10 °C for 70 h. This ultracentrifugation at a slightly higher density enabled separation of the various aggrecan populations. The solution in the tube was fractionated into nine tubes (D1–D9) from the bottom. Aggrecan separation was monitored by immuno-dot blot analysis.

Immuno-dot Blot Analysis—The samples were applied to nylon N^+ membranes by dot blot using the BIO-DOT™ apparatus (Bio-Rad). The membranes were immunodetected as previously described with slight modification (4). They were pretreated with 1 unit/ml protease-free chondroitinase ABC (Seikagaku). For aggrecan core protein detection, rabbit polyclonal anti-aggrecan (×5000) and peroxidase-conjugated goat anti-rabbit IgG (×10,000; Cappel) were used as the primary and secondary antibodies, respectively.

Characterization of CS Chains—The transfected LTC cells were plated in a 100-mm culture dish. After 2 days, they were labeled with [^{35}S]sulfate (100 μCi/ml) for 24 h. The cells and conditioned medium were collected separately at day 3 and extracted with 0.2 M NaOH for 16 h at room temperature. Next, they were neutralized by the addition of 4 M acetate and digested with 1 mg/ml proteinase K in 50 mM Tris-HCl, pH 8.0, for 2 h at 37 °C. The samples were applied to a DEAE-Sephacel (Amersham Biosciences) column that was equilibrated with 50 mM Tris-HCl, pH 7.5. After washing with 10 column volumes of 50 mM Tris-HCl, pH 7.5, 0.2 M NaCl, glycosaminoglycan-rich fractions were eluted with 50 mM Tris-HCl, pH 7.5, 2 M NaCl. The eluates were precipitated by the addition of 3 volumes of 95% ethanol containing 1.3% potassium acetate, and the precipitate was dissolved in 1 ml of distilled water. A portion (100 μl) of the sample was further isolated by treatment with a mixture of 10 microunits/ml heparitinase I (Seikagaku), 5 microunits/ml, heparitinase II (Seikagaku), and 10 microunits/ml heparinase (Seikagaku) in 20 mM acetate buffer, pH 7.0, 2 mM calcium acetate for 2 h at 37 °C. Separation was performed using an Ultrafree-MC filter cup (Millipore) and dissolved in 200 μl of distilled water. To evaluate [^{35}S]sulfate incorporation, a portion (100 μl) of the sample was measured by scintillation counting. To examine the chain lengths, the other portion (100 μl) of the

sample was applied to a Superose 6 column (Amersham Biosciences) equilibrated in 50 mM Tris-HCl, pH 7.5, and 0.2 M NaCl. Elution of the CS chains was monitored by scintillation counting. In separate experiments, heparitinase-resistant glycosaminoglycan fractions were prepared from the conditioned medium of nonlabeled LTC cells as described above. The sample was labeled with ^{3}H-labeled sodium borohydride as described previously (27). After the removal of free ^{3}H-labeled sodium borohydride using a Sephadex G-25 spin column, the labeled sample (~90,000 cpm) was applied to a Superose 6 column under the same conditions as above.

Analysis of CS Disaccharide Composition—Transfected LTC cells were plated in a 100-mm culture dish. The cells and conditioned medium were collected separately at day 2. Glycosaminoglycans were isolated by β-elimination, protease digestion, and DEAE-Sephacel column chromatography, as described above. The eluates were precipitated by the addition of 3 volumes of 95% ethanol containing 1.3% potassium acetate, and the precipitate was dissolved in 100 μl of distilled water. The samples were treated with 30 milliunits of chondroitinase ABC in 25 μl of 50 mM Tris-HCl, pH 7.5, 0.04% bovine serum albumin for 2 h at 37 °C, and filtered using Ultrafree-MC (5,000 molecular weight limit). Unsaturated disaccharides in the filtrates were analyzed by reverse phase ion pair chromatography using the Senshu Pak column Docosil with a fluorescence detector according to Toyoda's method (28) with a slight modification of elution conditions. The modified gradient program was as follows: 0–10 min, 1–4% eluent B; 10–11 min, 4–10% eluent B; 11–20 min, 10–18% eluent B; 20–22 min, 18–70% eluent B; 22–29 min, 70% eluent B.

Construction of the CSGalNAcT-1 Adenovirus Expression Vector, Viral Particle Production, and in Vivo Transduction to Vertebral Disc—cDNA encoding human CSGalNAcT-1 was prepared by PCR using the primers (5′-CACCATGATGATGGTTCGCCG-3′, 5′-TGTTTTTTTGCTACTTGTCTTCTG-3′) and CSGalNAcT-1/pcDNA3.1(+) as the template. This cDNA was then subcloned into pAd/CMV/V5-DEST (Invitrogen) using pENT/D-TOPO (Invitrogen). Adenoviral particles were obtained by transfecting 293A cells with the CSGalNAcT-1 adenoviral expression plasmid, and the titer was checked according to the manufacturer's instructions (ViraPower™ adenoviral expression system; Invitrogen). Adenoviral particles prepared using pAd/CMV/V5-GW/Lac-Z (Invitrogen) were used as the negative control. The particles (1.5×10^7 plaque-forming units) were injected into the caudal intervertebral discs of 4-month-old ICR mice. One week after the injection, the mice were sacrificed, and the caudal vertebrae were immersed in 4% paraformaldehyde at 4 °C overnight and decalcified with K-CX solution (Fujisawa) for 24 h at room temperature. The samples were then embedded in paraffin and sliced into 4-μm sections.

RESULTS

Expression Patterns of Glycosyltransferases Involved in CS Biosynthesis in Cartilage—The growth plate cartilage contains chondrocytes at different stages of differentiation: resting, proliferative, prehypertrophic, and hypertrophic chondrocytes (29). During differentiation, chondrocytes at the prehypertrophic stage show the highest level of aggrecan synthesis (30). Since the CS chains are attached to the core protein of aggrecan in cartilage, the expression of the key enzymes required for CS biosynthesis is probably up-regulated, correlating with the expression of aggrecan core protein during chondrocyte differentiation. Initially, we investigated the expression of glycosyltransferases involved in CS biosynthesis in mouse developing cartilage. By *in situ* hybridization, CSS-1, CSS-2, CSGlcAT, and CSGalNAcT-1 were shown to be expressed in the prehypertrophic zone of the growth plate at E16.5, colocalized with aggrecan core protein. In particular, CSGalNAcT-1 was expressed at the highest level. In contrast, CSS-3 and CSGalNAcT-2 were expressed at very low levels (Fig. 2).

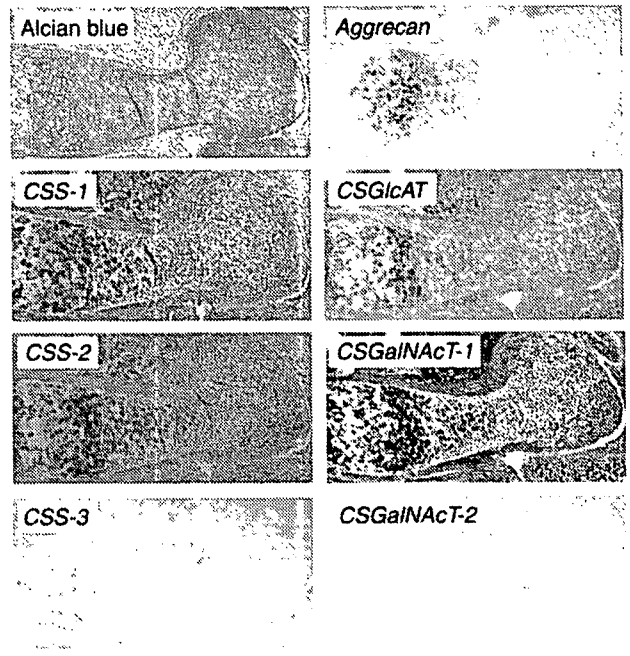

FIGURE 2. ***In situ* hybridization patterns of the glycosyltransferases involved in CS biosynthesis and aggrecan core protein in developing cartilage.** The expression patterns of aggrecan core protein (*Aggrecan*), CSS-1, CSS-2, CSS-3, CSGlcAT, and CSGalNAcT-1 and -2 in a mouse humerus at E16.5 are shown together with the staining pattern with Alcian blue. Note that CSS-1, CSS-2, CSGlcAT, and CSGalNAcT-1 are expressed in the prehypertrophic zone of the growth plate at E16.5 and colocalized with aggrecan core protein. CSGalNAcT-1, in particular, showed the highest level of expression.

Next, we examined the expression patterns of the CS biosynthetic enzymes in ATDC5 cells, which reflect the *in vivo* chondrocyte differentiation process (24, 31). The expression of both CSGlcAT and CSGalNAcT-1 was increased similar to that of aggrecan core protein, whereas response was less pronounced for that of CSS-1, CSS-2, and CSGalNAcT-2. The expression of CSS-3 was not detected (Fig. 3). Another chondrogenic cell line N1511 (25) displayed expression patterns similar to those of CS biosynthetic enzymes during differentiation (data not shown). These *in vitro* cell culture results indicate that the expression of CSGlcAT and CSGalNAcT-1 correlates well with that of aggrecan core protein.

Real time RT-PCR showed a high level of CSGalNAcT-1 expression and lower levels of CSS-1, CSS-2, and CSGlcAT expression in cartilage at E18.5 (Fig. 4*B*, *open bar*); this is consistent with the *in situ* hybridization data. We further

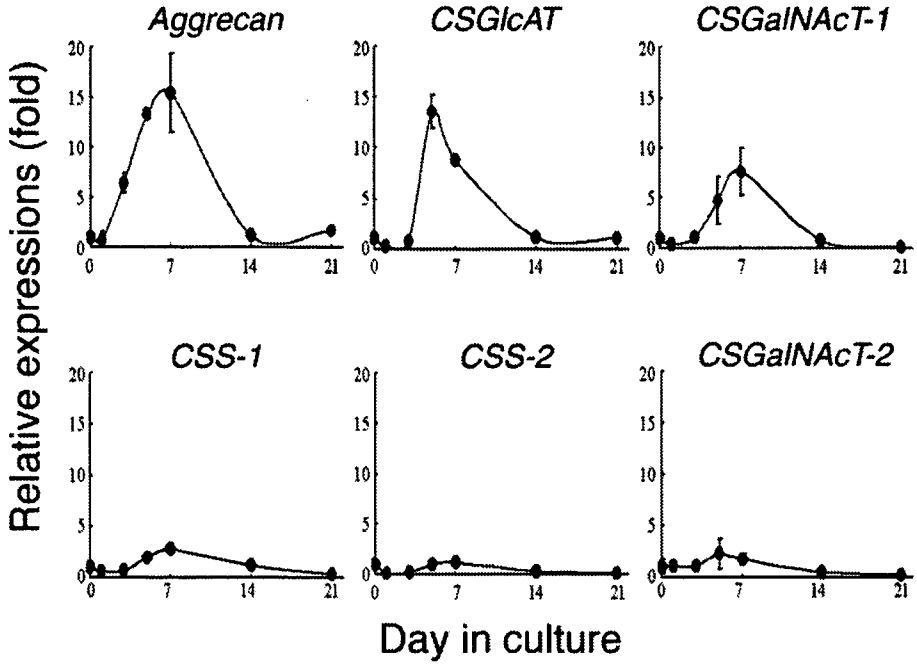

FIGURE 3. **Expression patterns of the glycosyltransferases involved in CS biosynthesis during chondrocyte differentiation of the ATDC5 cells.** The expression levels were standardized with those of glyceraldehyde-3-phosphate dehydrogenase and plotted as a -fold increase against the level at confluence (day 0). Note the correlated expression of CSGlcAT and CSGalNAcT-1 with that of aggrecan core protein.

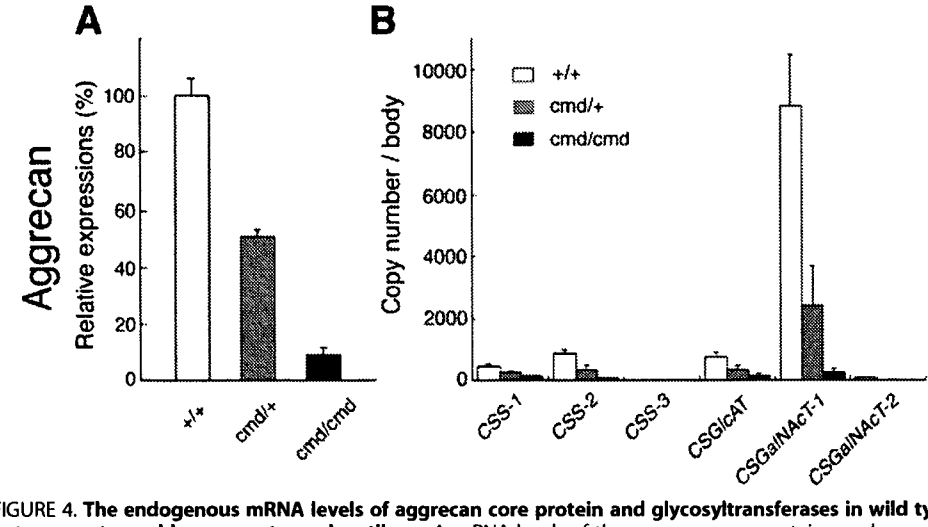

FIGURE 4. **The endogenous mRNA levels of aggrecan core protein and glycosyltransferases in wild type, heterozygote, and homozygote cmd cartilage.** *A*, mRNA levels of the aggrecan core protein are shown as a percentage of wild type E18.5 cartilage. *B*, mRNA levels of glycosyltransferases are shown as the copy number (+/+, wild type; *cmd/+*, heterozygote cmd; *cmd/cmd*, homozygote cmd). Note the high expression of CSGalNAcT-1 and its good correlation with that of aggrecan core protein.

investigated the correlation between CS biosynthetic enzymes and aggrecan expression, using cartilage isolated from mice with cmd, known as natural aggrecan-null mice (32, 33). Since the heterozygote and homozygote cmd cartilage exhibited ~50 and ~9% aggrecan gene transcription, respectively (Fig. 4*A*), quantification of the enzyme expression in the wild type, heterozygote, and homozygote cartilage could facilitate the identification of enzymes critical for CS biosynthesis. In the cmd heterozygote cartilage, CSGalNAcT-1 expression was diminished to ~30% that of the wild type, whereas expression of the other enzymes was constantly low (Fig. 4*B*, *gray bar*). In the cmd homozygote cartilage, CSGalNAcT-1 expression further decreased to a low level similar to that of the other enzymes (Fig. 4*B*, *black bar*). These results, demonstrating high levels of gene expression in cartilage and a good correlation with aggrecan core protein expression, suggested that CSGalNAcT-1 mainly regulates CS synthesis in cartilage.

CSGalNAcT-1 Overexpression Enhances CS Biosynthesis in Chondrocytic Cells—Next, we examined whether CSGalNAcT-1 overexpression could enhance CS biosynthesis in LTC cells. LTC cells are derived from a rat chondrosarcoma and have the characteristics of mature chondrocytes, including a high level of aggrecan expression (34, 35). Cells stably transfected with the CSGalNAcT-1 expression plasmid overexpressed human CSGalNAcT-1 mRNA by ~80-fold compared with endogenous rat mRNA expression (data not shown). Metabolic labeling with [^{35}S]sulfate showed up to a ~2.2-fold increase in CS levels in both the conditioned medium and the cell lysates of the CSGalNAcT-1-overexpressing cells compared with the mock-transfected cells. In contrast, stable clones overexpressing comparable levels of CSS-1, CSS-2, and CSGlcAT did not show increased CS biosynthesis (Fig. 5*A*). A stronger staining intensity with Alcian blue confirmed the increased CS biosynthesis in the CSGalNAcT-1-overexpressing cells (Fig. 5*B*). These results indicate that, whereas the activity of CSS-1, CSS-2, and CSGlcAT in LTC cells is saturated, that of CSGalNAcT-1 is not and that CSGalNAcT-1 overexpression further enhances CS biosynthesis.

Aggrecan in CSGalNAcT-1-overexpressing Cells Contains a Larger Number of CS Chains—Aggrecan core protein expression may have been up-regulated by CSGalNAcT-1 overexpression, as shown by the correlation between the expression in ATDC5 and N1511 cells and that in cmd cartilage. However, real time RT-PCR revealed similar mRNA levels of aggrecan core protein in both CSGalNAcT-1 and mock-transfected LTC cells (Fig. 6*A*). Dot blot analysis showed similar levels of aggrecan core protein in the conditioned media and cell lysates of both transfected cell types (Fig. 6*B*). Since these data suggested that aggrecan synthesized in the CSGalNAcT-1-overexpressing cells contains a larger CS amount per molecule, we examined the density of aggrecan. CsCl density gradient ultracentrif-

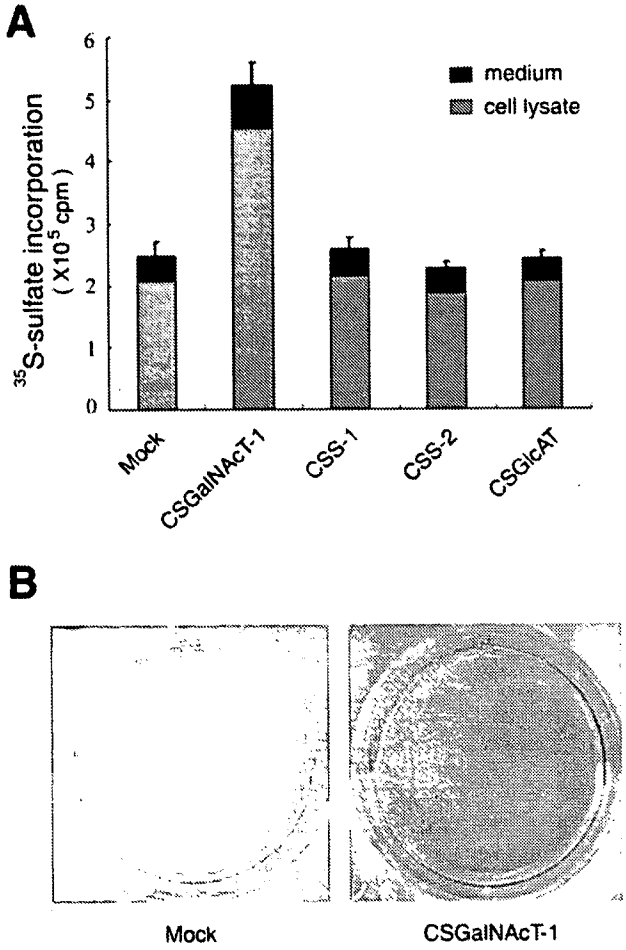

FIGURE 5. **Increased CS levels following the overexpression of CSGalNAcT-1 in LTC cells.** Stable transfectants overexpressing CSGalNAcT-1, CSS-1, CSS-2, CSGlcAT, and mock transfectants were established by transfecting LTC cells with expression vectors of the enzyme genes followed by selection with G418 for 10 days. *A*, [^{35}S]sulfate incorporation of mock-transfected cells and CSGalNAcT-1-, CSS-1-, CSS-2-, and CSGlcAT-overexpressing cells is shown (*gray bar*, cell lysates; *black bar*, conditioned medium). Note that CSGalNAcT-1-overexpressing cells exhibit an ~2.2-fold increase in CS biosynthesis compared with the mock-transfected cells, whereas the others do not. *B*, culture plates stained with Alcian blue (pH 1.0). CSGalNAcT-1-overexpressing cells exhibited a stronger staining intensity than the mock-transfected cells.

ugation followed by dot blot detection of aggrecan core protein showed that aggrecan obtained from the CSGalNAcT-1-overexpressing cells was present in the bottom fractions, whereas aggrecan from the mock-transfected cells was widely distributed (Fig. 6*C*). Immunohistochemically, CS stained stronger in the pericellular zone of the CSGalNAcT-1-overexpressing cells than in the mock-transfected cells, whereas aggrecan core protein stained at similar levels (Fig. 6*D*). These observations indicate that aggrecan in the CSGalNAcT-1-overexpressing cells contains a larger amount of CS.

The increased amounts of CS imply that there is an increased number of CS chains or greater elongation of individual CS chains in GSGalNAcT-1-transfected cells. To examine CS chain length, we performed metabolic labeling of the CS chains synthesized in the transfected cells and subjected them to gel chromatography. The elution profile demonstrated CS chains with peaks at the same position (Fig. 7*A*, *arrows*). Furthermore, direct molecular sieve analysis of ^{3}H-labeled CS chains confirmed the same size of CS chains (Fig. 7*B*). These results indicate that the CS chain length in GSGalNAcT-1 and mock-transfected cells was similar, although there was an ~2.2-fold increase in CS incorporation in the CSGalNAcT-1-overexpressing cells. The functions of the CS chains, such as water absorption, depend on their saccharide structure, including sulfation (36). When the CS disaccharide composition was analyzed, a similar ratio of hexuronic acid (HexA)-GalNAc, HexA-GalNAc(4S), and the other disaccharides was observed in both the GSGalNAcT-1- and mock-transfected cells (9.9, 88.2, and 1.9% for mock; 4.3, 93.6, and 2.1% for CSGalNAcT-1-overexpressing cells) (Fig. 7*C*). Therefore, CSGalNAcT-1 overexpression appeared to cause a 2.2-fold increase in the number of CS chains along with a similar sulfation level per chain.

In Vivo Gene Delivery of CSGalNAcT-1 Increases CS Biosynthesis in Cartilage—Our *in vitro* studies using cell lines demonstrated that CSGalNAcT-1 overexpression increases CS biosynthesis. Since chondrocytes *in vivo* may utilize a similar mechanism, we tested whether *in vivo* gene delivery of CSGalNAcT-1 increases CS biosynthesis in cartilage. A replication-deficient adenovirus 5 containing a cDNA encoding CSGalNAcT-1 and the V5 epitope tag was injected into the nucleus pulposus of the intervertebral discs of 4-month-old mice, and its expression was confirmed by immunostaining for the V5 tag (data not shown). Histological analysis at day 7 after the injection showed intense Alcian blue staining in the pericellular zone of the nucleus pulposus cells in the disc and chondrocytes in the vertebral endplate compared with mice injected with the control adenovirus (Fig. 8). These results demonstrated that *in vivo* gene delivery of CSGalNAcT-1 in fact increased CS biosynthesis in cartilage.

DISCUSSION

In this study, we identified CSGalNAcT-1 as a key enzyme for CS biosynthesis in cartilage. Analysis of the expression patterns of glycosyltransferases and aggrecan core protein in normal developing cartilage by *in situ* hybridization, in chondrogenic cell lines, and in the aggrecan-null cartilage of cmd mice demonstrated both high level expression of CSGalNAcT-1 and good correlation of its expression with that of aggrecan core protein. Furthermore, CSGalNAcT-1 overexpression in cultured chondrocytic cells and the intervertebral disc elevated CS synthesis in the cells. These observations suggest that CSGalNAcT-1 is still unsaturated in chondrocytes, and an increase in the level of CS via its overexpression leads to prevention of cartilage destruction.

Of the six glycosyltransferases involved in CS biosynthesis, CSGalNAcT-1 expression was the highest in E18.5 mouse cartilage exhibiting ~170-fold higher expression than that of CSGalNAcT-2 (Fig. 4*B*). In tissues other than cartilage, CSGalNacT-1 is expressed at the highest level in the thyroid gland and placenta, which exhibit expression only up to 1.5–5-fold that of CSGalNAcT-2 (20). In addition, various cell lines show relatively low levels of CSGalNAcT-1 expression compared with other enzymes (18).[3] Thus, the high expression of CSGalNAcT-1 appears to be characteristic of chondrocytes and car-

[3] K. Sakai, unpublished data.

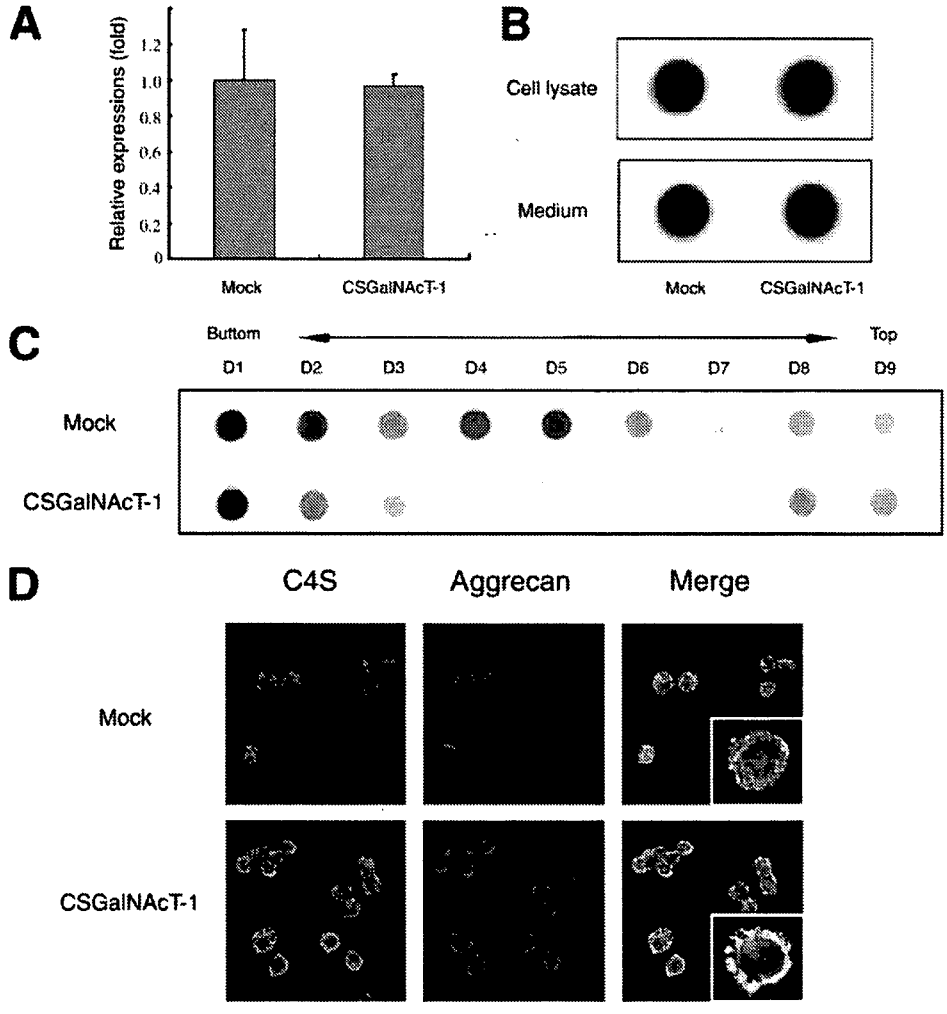

FIGURE 6. **Characterization of aggrecan in CSGalNAcT-1-overexpressing cells.** The aggrecan in CSGalNAcT-1-overexpressing cells contains a large amount of CS. *A*, mRNA levels of aggrecan core protein measured by real time RT-PCR. *B*, immunoblot of aggrecan core protein in cell lysates and conditioned medium. *C*, immunoblot analysis of aggrecan core protein after CsCl density gradient ultracentrifugation. Note that aggrecan in CSGalNAcT-1-overexpressing cells is mainly present in the bottom fractions (fractions 1 and 2), whereas that in mock-transfected cells is widely distributed in fractions 1–6. The density (g/ml) of each fraction is 1.638 for D1, 1.615 for D2, 1.600 for D3, 1.573 for D4, 1.525 for D5, 1.512 for D6, 1.465 for D7, 1.460 for D8, and 1.420 for D9, respectively. *D*, immunostaining for aggrecan core protein and chondroitin 4-sulfate (*C4S*). Chondroitin 4-sulfate stains stronger in the pericellular zone of CSGalNAcT-1-overexpressing cells than in the mock-transfected cells, whereas the aggrecan core protein stained at similar levels.

tilage. CSGalNAcT-1 expression correlated well with that of aggrecan core protein that provides acceptor sites for the glycosaminoglycan chains. CSGalNAcT-1 expression was closely associated with chondrocyte differentiation. Since CSGalNAcT-1 expression was diminished accordingly in the heterozygote and homozygote cmd cartilage, the expression of aggrecan core protein may regulate that of CSGalNAcT-1. Aggrecan core protein as substrate may be required for enzyme complex, and its decrease may deliver a feedback signal toward down-regulation of CSGalNAcT-1 expression. Alternatively, aggrecan in the cartilage matrix may maintain the chondrocyte phenotype, including high level expression of CSGalNAcT-1. Thus far, we have not identified *cis*-elements that are specific to chondrocyte differentiation in the promoter region of the CSGalNAcT-1 gene. The transcriptional regulation of this gene remains to be studied.

We demonstrated the presence of aggrecan with a larger number of attached CS chains in CSGalNAcT-1-overexpressing cells (Fig. 9). We designate this molecule "superaggrecan," since it would more efficiently contribute to cartilage function. Since CSGalNAcT-1 has stronger initiating activity than elongating activity (18), chain initiation may be the rate-limiting step in CS biosynthesis, and chondrocytes may have sufficient machinery for CS chain elongation following initiation. Indeed, overexpression of CSS-1, CSS-2, and CSGlcAT did not increase CS biosynthesis. The other enzyme involved in chain initiation, CSGalNAcT-2, showed consistent low expression in cartilage and has lower initiation activity than CSGalNAcT-1 (20), excluding any major involvement in cartilage CS biosynthesis. Enhanced CS biosynthesis by CSGalNAcT-1 overexpression suggests the presence of a large number of linkage regions as acceptor substrates in the native aggrecan. Although the aggrecan core protein has more than 100 putative Ser-Gly sequences of the CS attachment sites (2), approximately half of them may be attached only with the linkage tetrasaccharides. However, stubs of the linkage region have not been identified in aggrecan, although such stubs are present in a part-time CS proteoglycan thrombomodulin, an integral membrane glycoprotein expressed on endothelial cell surfaces (37). Recently, GlcAT-I, which transfers a GlcUA residue to the second Gal residue in the linkage region, has been shown to increase CS biosynthesis to ~1.5-fold (38). Thus, an immature linkage region may be present, and the enzyme complex that includes GlcAT-I and CSGalNAcT-1 may catalyze the completion of the linkage region and CS chain initiation.

Lines of evidence that support CSGalNAcT-1 as the critical enzyme for CS biosynthesis in various tissues as well as cartilage have been presented. Syndecan-4 in CSGalNAcT-1-overexpressing COS7 cells contains a large amount of CS (20). CSGalNAcT-1 overexpression in Balb/3T3 cells, a cell line established from normal mouse fibroblast cells, achieves ~5-fold CS synthesis.[3] Taken together, these observations strongly suggest that chain initiation by CSGalNAcT-1 is a critical step in the regulation of CS biosynthesis, and overexpression of the enzyme would substantially increase CS synthesis in various tissues.

To date, many approaches to promote cartilage regeneration have been attempted, including the treatment of mes-

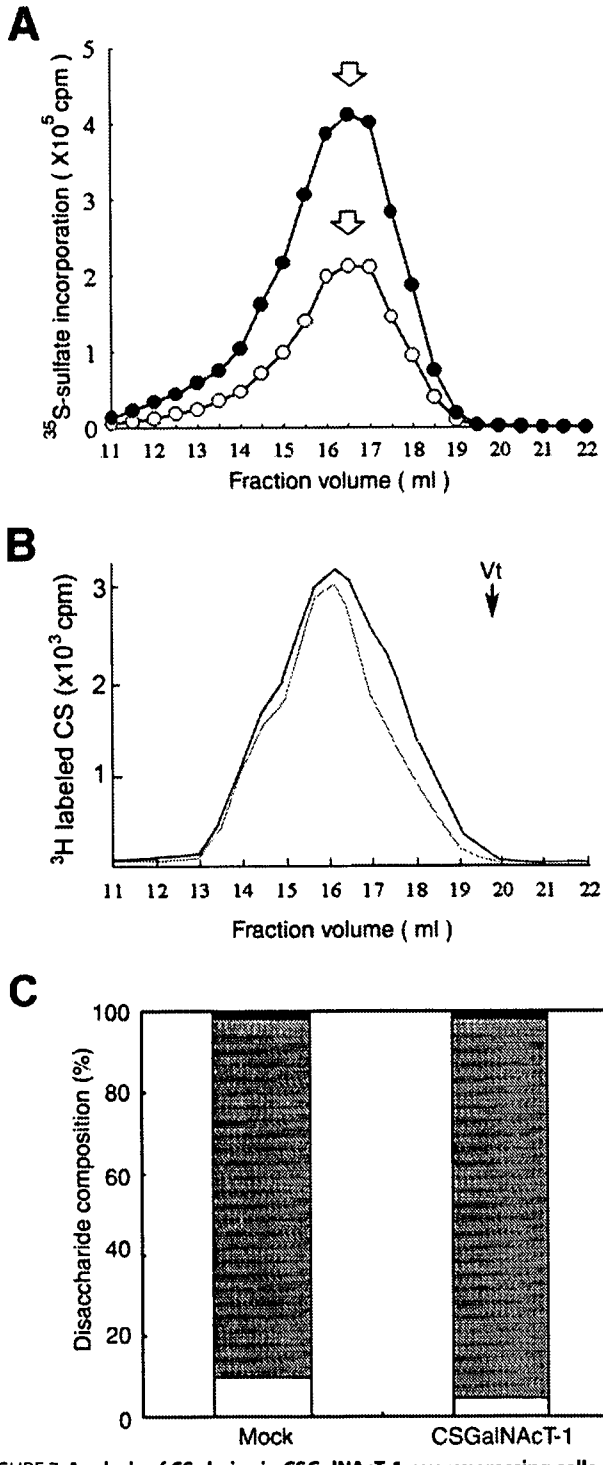

FIGURE 7. **Analysis of CS chains in CSGalNAcT-1-overexpressing cells.** *A*, elution profiles of Superose 6 gel chromatography. The cells were metabolically labeled with [^{35}S]sulfate for 24 h. Glycosaminoglycans, extracted as indicated under "Experimental Procedures," were applied to the Superose 6 column. The samples from CSGalNAcT-1-overexpressing cells (*closed circle*) and the mock transfectant cells (*open circle*) are shown. Note that two peaks are located at the same position (*arrows*). *B*, elution profiles of Superose 6 gel chromatography. CS-rich fractions prepared from the conditioned medium were labeled with ^{3}H-labeled sodium borohydride and were applied to Superose 6 column. The samples from CSGalNAcT-1-overexpressing cells (*thick line*) and the mock-transfectant cells (*narrow line*) are shown. Note that two peaks are at the same position. *Vt*, position of the total volume. *C*, disaccharide composition of CS in CSGalNAcT-1 and mock transfectants. HexA-GalNAc (*open bar*), HexA-GalNAc(4S) (*gray bar*), and others (*black bar*) are shown as a percentage of the saccharide content. HexA-GalNAc, HexA-GalNAc(4S), and the other disaccharides were observed to have similar ratios in both GSGalNAcT-1- and mock-transfected cells.

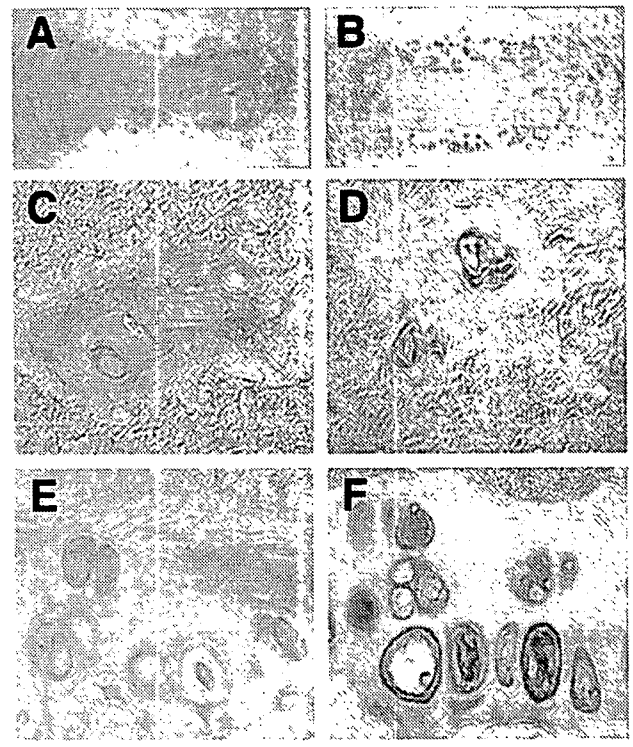

FIGURE 8. **Increased CS biosynthesis by *in vivo* gene delivery of CSGalNAcT-1.** Shown are histological sections of mouse intervertebral discs at 4 months of age, which were stained with Alcian blue (pH 1.0), 7 days after an injection of adenoviral particles. Low magnification of the intervertebral disc (*A* and *B*), higher magnification of nucleus pulposus (*C* and *D*), and the endplate (*E* and *F*) injected with mock (*A*, *C*, and *E*) and CSGalNAcT-1 (*B*, *D*, and *F*) adenovirus are shown. Note the intense Alcian blue staining in the pericellular zone of the nucleus pulposus cells in the disc and chondrocytes in the vertebral endplate of mice with CSGalNAcT-1 gene delivery compared with mice injected with the control adenovirus.

enchymal stem cells with growth factors to promote their differentiation into chondrocytes and the implantation of chondrocytes incorporated into scaffolds that maintain cellular phenotype and support the tissue structure (39–42). These interventions are based on the notion that aggrecan is synthesized only by chondrocytes and that it is essential for cartilage function. However, because of the difficulty in maintaining aggrecan synthesis in chondrocytes, regeneration of functional cartilage has not yet been achieved. In contrast to the above approaches, our research focused on CS as the critical factor that determines cartilage function and successfully generated superaggrecan. Since the turnover of aggrecan in cartilage is slow, with a half-life of approximately 10 years (43–45), the function of superaggrecan will most probably be maintained.

Adenoviral gene delivery of CSGalNAcT-1 enhanced *in vivo* CS synthesis in nucleus pulposus cells and endplate chondrocytes. In contrast, we have been unsuccessful in gene delivery to the articular cartilage (data not shown), although a recent similar study demonstrated increased CS expression in an articular cartilage explant (38). Since CS biosynthesis occurs in the Golgi apparatus (22), the addition of the enzyme to the tissue is ineffective, and overexpression in the cell is essential for this enzyme-based increase in CS levels. Effective gene delivery of CSGalNAcT-1 would be necessary to evaluate the prevention of cartilage destruction.

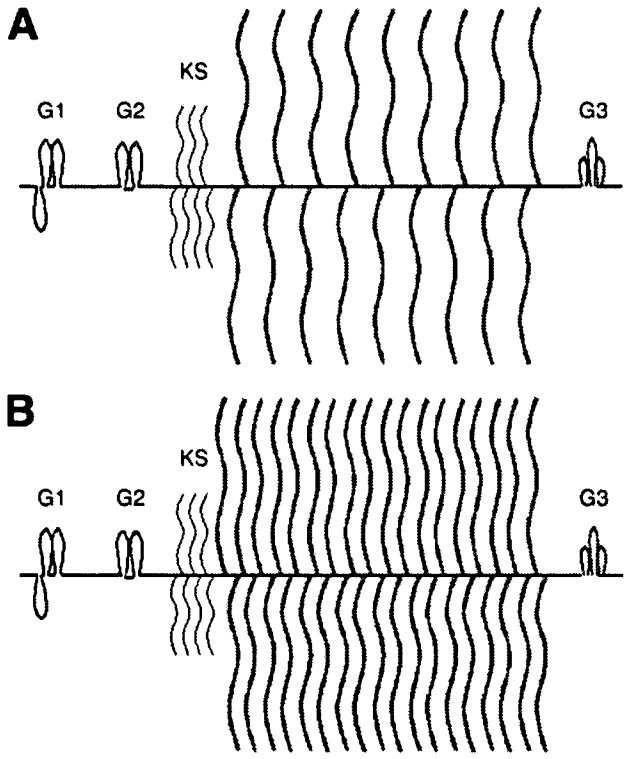

FIGURE 9. **A schematic diagram of aggrecan synthesized by control and CSGalNAcT-1-overexpressing chondrocytes.** *A*, native aggrecan; *B*, aggrecan in CSGalNAcT-1-overexpressing cells, which contains ~2.2-fold the number of CS chains attached to the core protein; designated "superaggrecan" (*blue*, CS chain). *G1*, G1 globular domain; *G2*, G2 globular domain; *G3*, G3 globular domain; *KS*, keratan sulfate.

In conclusion, this study identified the glycosyltransferase critical for CS biosynthesis and proposes a novel strategy for the treatment of cartilage degenerative disorders, distinct from cell-based approaches that focus on chondrocyte differentiation and aggrecan core protein expression. The effects of superaggrecan on chondrocyte homeostasis and its susceptibility to aggrecan-degrading proteinases remain to be performed.

Acknowledgments—We thank Dr. Rafrenie (Northern Ontario School of Medicine, Sudbury, Canada) for proofreading the manuscript, Drs. N. Sugiura and H. Habuchi for technical comments, Dr. H. Kitagawa for valuable discussion, and S. Hara for technical assistance.

REFERENCES

1. Watanabe, H., Yamada, Y., and Kimata, K. (1998) *J. Biochem. (Tokyo)* **124,** 687–693
2. Watanabe, H., Gao, L., Sugiyama, S., Doege, K., Kimata, K., and Yamada, Y. (1995) *Biochem. J.* **308,** 433–440
3. Doege, K. J., Garrison, K., Coulter, S. N., and Yamada, Y. (1994) *J. Biol. Chem.* **269,** 29232–29240
4. Plaas, A. H., Wong-Palms, S., Roughley, P. J., Midura, R. J., and Hascall, V. C. (1997) *J. Biol. Chem.* **272,** 20603–20610
5. Roughley, P., Martens, D., Rantakokko, J., Alini, M., Mwale, F., and Antoniou, J. (2006) *Eur. Cell. Mater.* **11,** 1–7
6. Bayliss, M. T. (1990) *Biochem. Soc. Trans.* **18,** 799–802
7. Dieppe, P. A., and Lohmander, L. S. (2005) *Lancet* **365,** 965–973
8. Creamer, P., and Hochberg, M. C. (1997) *Lancet* **350,** 503–508
9. Luoma, K., Riihimaki, H., Luukkonen, R., Raininko, R., Viikari-Juntura, E., and Lamminen, A. (2000) *Spine* **25,** 487–492
10. Andersson, G. B. (1999) *Lancet* **354,** 581–585
11. Silbert, J. E., and Sugumaran, G. (2002) *IUBMB Life* **54,** 177–186
12. Rohrmann, K., Niemann, R., and Buddecke, E. (1985) *Eur. J. Biochem.* **148,** 463–469
13. Kitagawa, H., Uyama, T., and Sugahara, K. (2001) *J. Biol. Chem.* **276,** 38721–38726
14. Kitagawa, H., Izumikawa, T., Uyama, T., and Sugahara, K. (2003) *J. Biol. Chem.* **278,** 23666–23671
15. Yada, T., Gotoh, M., Sato, T., Shionyu, M., Go, M., Kaseyama, H., Iwasaki, H., Kikuchi, N., Kwon, Y. D., Togayachi, A., Kudo, T., Watanabe, H., Narimatsu, H., and Kimata, K. (2003) *J. Biol. Chem.* **278,** 30235–30247
16. Yada, T., Sato, T., Kaseyama, H., Gotoh, M., Iwasaki, H., Kikuchi, N., Kwon, Y. D., Togayachi, A., Kudo, T., Watanabe, H., Narimatsu, H., and Kimata, K. (2003) *J. Biol. Chem.* **278,** 39711–39725
17. Gotoh, M., Yada, T., Sato, T., Akashima, T., Iwasaki, H., Mochizuki, H., Inaba, N., Togayachi, A., Kudo, T., Watanabe, H., Kimata, K., and Narimatsu, H. (2002) *J. Biol. Chem.* **277,** 38179–38188
18. Gotoh, M., Sato, T., Akashima, T., Iwasaki, H., Kameyama, A., Mochizuki, H., Yada, T., Inaba, N., Zhang, Y., Kikuchi, N., Kwon, Y. D., Togayachi, A., Kudo, T., Nishihara, S., Watanabe, H., Kimata, K., and Narimatsu, H. (2002) *J. Biol. Chem.* **277,** 38189–38196
19. Uyama, T., Kitagawa, H., Tamura Ji, J., and Sugahara, K. (2002) *J. Biol. Chem.* **277,** 8841–8846
20. Sato, T., Gotoh, M., Kiyohara, K., Akashima, T., Iwasaki, H., Kameyama, A., Mochizuki, H., Yada, T., Inaba, N., Togayachi, A., Kudo, T., Asada, M., Watanabe, H., Imamura, T., Kimata, K., and Narimatsu, H. (2003) *J. Biol. Chem.* **278,** 3063–3071
21. Uyama, T., Kitagawa, H., Tanaka, J., Tamura, J., Ogawa, T., and Sugahara, K. (2003) *J. Biol. Chem.* **278,** 3072–3078
22. Silbert, J. E., and Freilich, L. S. (1980) *Biochem. J.* **190,** 307–313
23. Watanabe, H., and Yamada, Y. (1999) *Nat. Genet.* **21,** 225–229
24. Atsumi, T., Miwa, Y., Kimata, K., and Ikawa, Y. (1990) *Cell Differ. Dev.* **30,** 109–116
25. Kamiya, N., Jikko, A., Kimata, K., Damsky, C., Shimizu, K., and Watanabe, H. (2002) *J. Bone. Miner. Res.* **17,** 1832–1842
26. Matsumoto, K., Kamiya, N., Suwan, K., Atsumi, K., Shimizu, K., Shinomura, T., Yamada, Y., Kimata, K., and Watanabe, H. (2006) *J. Biol. Chem.* **281,** 18257–18263
27. Nogami, H., Suzuku, H., Habuchi, H., Ishiguro, N., Iwata, H., and Kimata, K. (2004) *J. Biol. Chem.* **279,** 8219–8229
28. Toyoda, H., Kinoshita-Toyoda, A., and Selleck, S. B. (2000) *J. Biol. Chem.* **275,** 2269–2275
29. DeLise, A. M., Fischer, L., and Tuan, R. S. (2000) *Osteoarthritis Cartilage* **8,** 309–334
30. Shibata, S., Fukada, K., Imai, H., Abe, T., and Yamashita, Y. (2003) *J. Anat.* **203,** 425–432
31. Shukunami, C., Shigeno, C., Atsumi, T., Ishizeki, K., Suzuki, F., and Hiraki, Y. (1996) *J. Cell Biol.* **133,** 457–468
32. Watanabe, H., Kimata, K., Line, S., Strong, D., Gao, L. Y., Kozak, C. A., and Yamada, Y. (1994) *Nat. Genet.* **7,** 154–157
33. Watanabe, H., Nakata, K., Kimata, K., Nakanishi, I., and Yamada, Y. (1997) *Proc. Natl. Acad. Sci. U. S. A.* **94,** 6943–6947
34. Choi, H. U., Meyer, K., and Swarm, R. (1971) *Proc. Natl. Acad. Sci. U. S. A.* **68,** 877–879
35. Oegema, T. R., Jr., Hascall, V. C., and Dziewiatkowski, D. D. (1975) *J. Biol. Chem.* **250,** 6151–6159
36. Silbert, J. E. (1996) *Glycoconj. J.* **13,** 907–912
37. Nadanaka, S., Kitagawa, H., and Sugahara, K. (1998) *J. Biol. Chem.* **273,** 33728–33734
38. Venkatesan, N., Barre, L., Benani, A., Netter, P., Magdalou, J., Fournel-Gigleux, S., and Ouzzine, M. (2004) *Proc. Natl. Acad. Sci. U. S. A.* **101,** 18087–18092
39. Martinek, V., Ueblacker, P., and Imhoff, A. B. (2003) *J. Bone Joint. Surg. Br.* **85,** 782–788
40. Kuo, C. K., Li, W. J., Mauck, R. L., and Tuan, R. S. (2006) *Curr. Opin. Rheumatol.* **18,** 64–73

41. Masuda, K., Oegema, T. R., Jr., and An, H. S. (2004) *Spine* **29,** 2757–2769
42. Anderson, D. G., Albert, T. J., Fraser, J. K., Risbud, M., Wuisman, P., Meisel, H. J., Tannoury, C., Shapiro, I., and Vaccaro, A. R. (2005) *Spine* **30,** S14–S19
43. Maroudas, A., Bayliss, M. T., Uchitel-Kaushansky, N., Schneiderman, R., and Gilav, E. (1998) *Arch. Biochem. Biophys.* **350,** 61–71
44. Sivan, S. S., Tsitron, E., Wachtel, E., Roughley, P. J., Sakkee, N., van der Ham, F., Degroot, J., Roberts, S., and Maroudas, A. (2006) *J. Biol. Chem.* **281,** 13009–13014
45. Maroudas, A. (1975) *Philos. Trans. R. Soc. Lond. B Biol. Sci.* **271,** 293–313

THE JOURNAL OF BIOLOGICAL CHEMISTRY VOL. 282, NO. 27, pp. 19589–19597, July 6, 2007

Essential Role of Heparan Sulfate 2-*O*-Sulfotransferase in Chick Limb Bud Patterning and Development*[S]

Received for publication, November 20, 2006, and in revised form, May 4, 2007 Published, JBC Papers in Press, May 10, 2007, DOI 10.1074/jbc.M610707200

Takashi Kobayashi[‡], Hiroko Habuchi[‡], Koji Tamura[§], Hiroyuki Ide[§], and Koji Kimata[‡1]

From the [‡]Institute for Molecular Science of Medicine, Aichi Medical University, Nagakute, Aichi 480-1195, Japan and [§]Department of Developmental Biology and Neurosciences, Graduate School of Life Sciences, Tohoku University, Aobayama Aobaku, Sendai 980-8578, Japan

The interactions of heparan sulfate (HS) with heparin-binding growth factors, such as fibroblast growth factors (FGFs), depend greatly on the chain structures. *O*-Sulfations at various positions on the chain are major factors determining HS structure; therefore, *O*-sulfation patterns may play a crucial role in controlling the developmental and morphogenetic processes of various tissues and organs by spatiotemporally regulating the activities of heparin-binding growth factors. In a previous study, we found that HS-2-*O*-sulfotransferase is strongly expressed throughout the mesoderm of chick limb buds during the early stages of development. Here we show that inhibition of HS-2-*O*-sulfotransferase in the prospective limb region by small inhibitory RNA resulted in the truncation of limb buds and reduced *Fgf-8* expression in the apical ectodermal ridge. The treatment also reduced *Fgf-10* expression in the mesenchyme. Moreover 2-*O*-sulfated HS, normally abundant in the basement membranes and mesoderm under ectoderm in limb buds, was significantly reduced in the treated buds. Phosphorylation levels of ERK and Akt were up-regulated in such truncated buds. Thus, we have shown for the first time that 2-*O*-sulfation of HS is essential for the FGF signaling required for limb bud development and outgrowth.

Chick limb bud is a useful model of limb pattern formation, which involves various growth factors and morphogens such as fibroblast growth factor (FGF),[2] hedgehog, wingless/Wnt, and bone morphogenetic proteins (1–4). Limb bud initiation requires reciprocal interactions between a specialized ectodermal structure called the apical ectodermal ridge (AER) and the underlying mesoderm (5, 6). At the time of limb initiation, in stages 13–15 of the chick embryo, *Fgf-8* in the intermediate mesoderm induces *Fgf-10* expression in the lateral plate mesoderm (LPM) of the prospective limb region. FGF-10 produced in the prospective limb mesoderm then induces *Fgf-8* expression in the overlying surface ectoderm (AER). FGF-8 secreted from AER maintains *Fgf-10* expression in the underlying mesoderm. This FGF signaling loop establishes the maintenance of AER and outgrowth of limb buds. FGF-8 also contributes to *Shh* induction, which in turn induces *Fgf-4* expression in the AER and maintains AER function in the posterior underlying mesoderm called the zone of polarizing activity (7, 8).

Although growth factors and morphogens are required for limb bud development and patterning, it is unclear how their signaling and distribution are regulated. Heparan sulfate proteoglycans, which are ubiquitous on the cell surface and in the extracellular matrix including basement membranes, are important regulators of such growth factor signaling and distribution (9–11). For example, chicken syndecan-3 is expressed throughout the distal mesenchymal cells and plays a role in limb bud outgrowth by controlling FGF signaling between the AER and mesoderm (12). Heparan sulfate proteoglycans play such roles by interacting with these growth factors (13–15); however, it is unclear what role HS chains play in these processes, although HS chains are known to interact with a variety of heparin-binding growth factors (HBGFs) such as FGF.

In FGF signaling, the ternary complex composed of HS chains, FGF family molecules, and FGF receptors (FGFRs) is formed on the cell surface (16–18). Specificities of interactions between heparan sulfate proteoglycan and ligand molecules are thought to reside in the fine structures of HS chains with specific sequences consisting of highly sulfated monosaccharides (*N*-, 2-*O*-, and/or 6-*O*-sulfated) (9, 19, 20). In fact, the different *O*-sulfation patterns of HS chains are involved in interactions with FGF family molecules (21–23). These fine structures are generated by the following modification reactions with specific enzymes after the backbone chain of HS is synthesized by the addition of alternating D-glucuronic acid and *N*-acetyl-D-glucosamine (GlcNAc) residues from the respective UDP sugars by EXT family proteins (24): GlcNAc *N*-deacetylation and *N*-sulfation by *N*-deacetylase/*N*-sulfotransferase, C-5 epimerization of D-glucuronic acid residues to iduronic acid by C-5 epimerase, and *O*-sulfations at various places that take place first at C-2 of IdoA and D-glucuronic acid by heparan sulfate 2-*O*-sulfotransferase (HS2ST), subsequently at C-6 of GlcNAc and *N*-sulfate-

* This work was supported by Grant-in-aid for Scientific Research on Priority Areas 14082206 from the Ministry of Education, Culture, Sports, Science and Technology of Japan and by a special research fund from the Seikagaku Corp. The costs of publication of this article were defrayed in part by the payment of page charges. This article must therefore be hereby marked "*advertisement*" in accordance with 18 U.S.C. Section 1734 solely to indicate this fact.

[S] The on-line version of this article (available at http://www.jbc.org) contains supplemental Fig. 1.

[1] To whom correspondence should be addressed. Tel.: 81-561-62-3311 (ext. 2088); Fax: 81-561-63-3532; E-mail: kimata@amugw.aichi-med-u.ac.jp.

[2] The abbreviations used are: FGF, fibroblast growth factor; HS, heparan sulfate; HS2ST, heparan sulfate 2-*O*-sulfotransferase; HS6ST, heparan sulfate 6-*O*-sulfotransferase; HBGF, heparin-binding growth factor; FGFR, fibroblast growth factor receptor; AER, apical ectodermal ridge; LPM, lateral plate mesoderm; RNAi, RNA interference; siRNA, small inhibitory RNA; esiRNA, endonuclease-digested small inhibitory RNA; ERK, extracellular signal-regulated kinase; pERK, phosphorylated ERK; pAkt, phosphorylated Akt; PBS, phosphate-buffered saline; GFP, green fluorescent protein; MAPK, mitogen-activated protein kinase; EXT, extosis.

D-glucosamine units by heparan sulfate 6-*O*-sulfotransferases (HS6STs), and lastly at C-3 of *N*-sulfate-D-glucosamine residues by heparan sulfate 3-*O*-sulfotransferases (25–27).

O-Sulfation residues and patterns have been shown to be critical to HS function in several developmental processes. For example, gene trap mutation of HS2ST in mice causes renal agenesis, eye and skeleton defects, and neonatal lethality (28). HS6ST-1 null mice die between embryonic day 15.5 and the perinatal stage and show a reduction in the number of fetal microvessels in the labyrinthine zone of the placenta (29). In addition, a recent report on mutant HS2ST and HS6ST-1 mice showed defects of specific axon guidance at the optic chiasm (30). Morpholino-mediated knockdown of HS6ST in zebrafish results in disruption of somitic muscle development and defects in the branching morphogenesis of the caudal vein (31, 32). Inhibition of *Drosophila* HS6ST expression by RNA interference (RNAi) reduces FGF signaling activity and disrupts the primary branching of the tracheal system (33).

Previously we showed distinctive expression patterns of HS *O*-sulfotransferases in developing chick limb buds (34). HS6ST-1 and HS6ST-2 transcripts are preferentially localized in the anterior and posterior proximal regions of the limb bud, respectively, whereas HS2ST transcripts are distributed rather uniformly throughout the bud. HS sulfation patterns in chick limb buds correspond exactly with these expression patterns (34). Thus, specific HS sulfation patterns may regulate the development and patterning of limb buds by binding to growth factors and morphogens. In this study, we examined the role of 2-*O*-sulfation in the morphogenesis of the chicken limb. Electroporation of RNA duplexes (RNAi technique) is effective at suppressing the expression of target genes in chick embryos (35). Disruption of the HS2ST gene by small inhibitory RNA (siRNA) reduced 2-*O*-sulfation levels and led to the abnormal development of limb buds, which showed less expression of both *Fgf-8* and *Fgf-10* accompanied by the up-regulation of phosphorylation of both ERK and Akt. Taken together, these results suggest that reducing 2-*O*-sulfate residues affect limb bud formation and outgrowth.

EXPERIMENTAL PROCEDURES

Preparation of Chicken Embryos—Fertile White Leghorn chicken eggs were obtained from Takeuchi Farm (Nara, Japan), incubated in humidified air at 38 °C, and staged according to Hamburger and Hamilton (36).

RNAi—Double-stranded RNA corresponding to the HS2ST open reading frame sequence was prepared and then digested with RNase III. Chicken HS2ST open reading frame was subcloned into pBluescriptII KS(−) (Stratagene, La Jolla, CA) before transcribing sense and antisense single-stranded RNA from T3 and T7 RNA polymerase promoters. RNA was incubated with DNase I to degrade the template DNA. Sense and antisense RNA were annealed into duplexes by combining equal amounts of each type of RNA, then denatured at 95 °C for 5 min, and incubated at 37 °C overnight. Annealed duplexes were incubated with RNase I (Ambion, Austin, TX) at 37 °C for 30 min and then treated with phenol-chloroform. The purified duplexes were resuspended in distilled water. To generate endonuclease-digested small inhibitory RNA (esiRNA), double-stranded RNA was incubated with RNase III (New England Biolabs, Beverly, MA) at 37 °C for 30 min. The reaction products were purified with siRNA Purification Units (Ambion), then precipitated with ethanol, and resuspended in distilled water. As controls for the siRNA treatment, siRNA mixtures for luciferase, the gene of which is derived from pGL3-Basic (Promega, Madison, WI), were prepared by the same procedure.

In Ovo Electroporation—For electroporation experiments, eggs were opened after 2 days of incubation at 38 °C, corresponding to stage 13-14, and a solution of India ink diluted in Tyrode's solution was applied below the blastoderm to enhance contrast. The vitellin membrane overlying the presumptive forelimb region was also carefully removed using a fine tungsten needle. RNA solutions containing 0–700 ng/μl esiRNA, 0.1% fast green, and 2 μg/μl pEGFP-N1 (Clontech) were injected into the LPM of the presumptive right forelimb region of embryos, and several drops of Tyrode's solution were added after injection. Electrodes were placed above (cathode) and below (anode) the forelimb region containing the injected RNA, and electroporation (three 15-V, 25-ms pulses) was performed with ElectroSquarePorator T820 (BTX; Inovio Biomedical Corp., San Diego, CA). Experimental embryos were observed and/or harvested 16–48 h after electroporation. For cryosections, embryos were fixed in 4% paraformaldehyde, PBS at 4 °C overnight and then incubated in 30% sucrose, PBS at 4 °C for 2–12 h. Embryos were embedded in OCT compound (Sakura, Tokyo, Japan), and 10-mm-thick cryosections were made.

In Situ Hybridization—Whole-mount and section *in situ* hybridization was performed as described previously with slight modifications (34, 37–39). For whole-mount *in situ* hybridization, embryos were fixed in 4% paraformaldehyde, PBS overnight and then digested with 1 μg/ml proteinase K in PBS containing 0.1% Tween 20 at 20 °C for 15 min. Hybridization was performed at 65 °C in 5× SSC, 50% (v/v) formamide, 1% (w/v) SDS, 50 μg/ml heparin, and 50 μg/ml yeast tRNA using digoxigenin-labeled RNA as a probe.

In Situ FGF-2 Binding Assay and Immunohistochemistry—For *in situ* detection of 2-*O*-sulfated HS, we used an exogenous FGF-2 binding assay (40). Cryosections were air-dried and then washed with PBS. To remove endogenous HS-bound molecules, sections were incubated with 2 M NaCl, PBS at room temperature for 10 min and then washed three times with PBS. When necessary, sections were treated with a mixture of heparitinases (Seikagaku Corp., Tokyo, Japan) at 37 °C for 2 h. Sections were incubated with 5–30 nM recombinant human FGF-2 (Roche Applied Science) at 4 °C overnight followed by blocking for 1 h at room temperature with PBS containing 10% bovine serum albumin (Sigma). After five washes with PBS, FGF-2 binding was analyzed using an anti-FGF-2 monoclonal antibody (05-118; Upstate Biotechnology, Lake Placid, NY) and Alexa-conjugated secondary antibody (Molecular Probes, Eugene, OR). HS was detected with 3G10 antibody (Seikagaku Corp.) and secondary antibody.

Western Blot Analysis—For Western blot analysis, tissue lysates of stage 22-23 limb buds were subjected to 10% SDS-polyacrylamide gel electrophoresis and transferred to a polyvinylidene difluoride membrane. The blots were incubated with

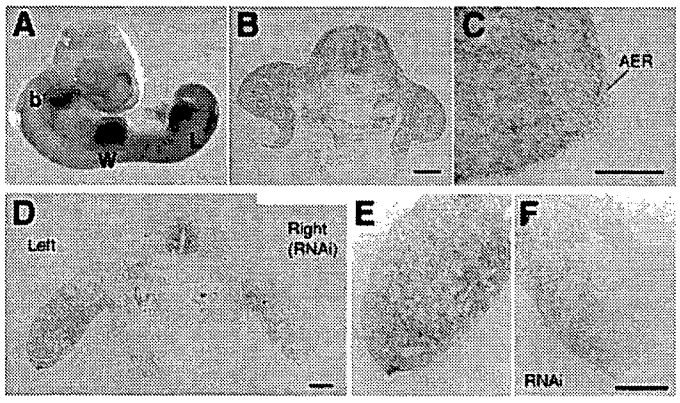

FIGURE 1. **Expression pattern of chicken HS2ST mRNA.** *A*, whole-mount *in situ* hybridization of stage 23 embryo. A high level of HS2ST transcripts was detected in wing (*W*) and leg (*L*) buds and in the branchial arches (*b*). *B* and *C*, *in situ* hybridization of transverse sections of stage 22 wing buds. HS2ST is expressed weakly in the AER and ectoderm (*C*). *D–F*, *in situ* hybridization of transverse sections of siRNA-injected embryos. HS2ST siRNA was injected into the prospective region of the right wing bud of stage 13 embryos (*D*). Treated embryos were fixed at stage 23-24 (45 h after treatment). The right bud (*F*) showed lower levels of HS2ST mRNA compared with the untreated left bud (*E*). *Scale bars* in *B*, *D*, and *F*, 200 μm; *scale bar* in *C*, 50 μm.

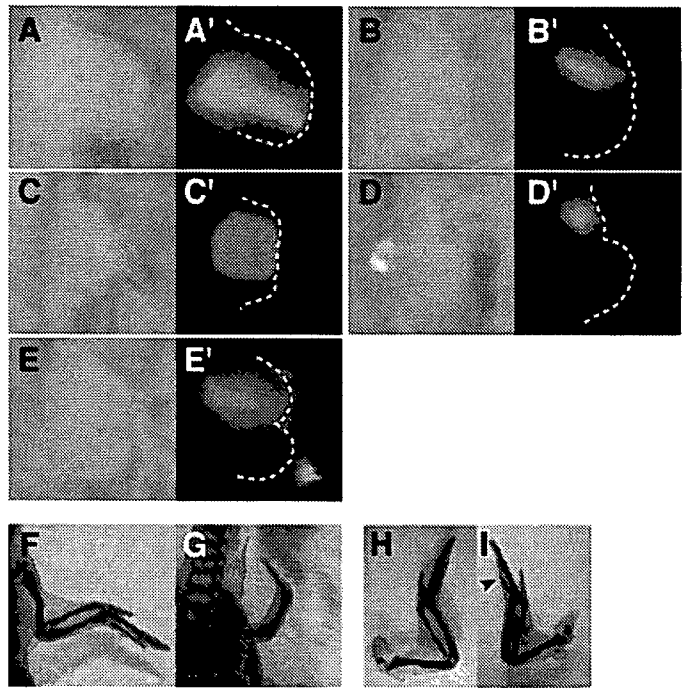

FIGURE 2. **Abnormal limb bud formation by HS2ST RNAi.** *A–E*, HS2ST esiRNA- or PBS-injected stage 22-23 limb bud. HS2ST siRNA mixtures (150 ng/μl) or PBS was injected, via electroporation, into the lateral plate mesoderm of the prospective right wing bud region of stage 13-14 embryos. *A'–E'*, GFP signals, derived from coelectroporated pEGFP-N1, indicated the siRNA-injected region. *A*, PBS-injected control samples had almost normal limb buds. *B–E*, HS2ST esiRNA-injected samples showed truncated limb buds. *B*, mildly truncated limb; *C*, moderately truncated limb; *D*, severely truncated limb; and *E*, indented limb. *F–I*, Alcian blue staining of skeletal patterns in HS2ST esiRNA-injected limbs revealed their abnormalities. *G*, severely affected right forelimb showing an abnormal skeletal pattern compared with untreated left forelimb (*F*). *I*, mildly affected right forelimb showing a defective digit (*arrowhead*) and size reduction compared with uninjected left forelimb (*H*).

10% skim milk in Tris-buffered saline/Tween 20 (TBST; Tris-buffered saline containing 0.1% Tween 20) and probed with anti-phosphorylated ERK (pERK) antibody (catalog number 9106; Cell Signaling Technology, Beverly, MA), anti-ERK antibody (catalog number 9102; Cell Signaling Technology), anti-phosphorylated Akt (pAkt) antibody (catalog number 9275; Cell Signaling Technology), or anti-actin antibody (catalog number A2066; Sigma) diluted with 1% skim milk in TBST. The signal was visualized using horseradish peroxidase-conjugated secondary antibody and enhanced chemiluminescence (Western Lighting Plus; PerkinElmer Life Sciences) according to the manufacturer's instructions.

Ligand and Carbohydrate Engagement Assays—In situ binding of the FGF·FGFR complex to heparan sulfate in the assay enables us to detect HS structure alterations (41, 42). The frozen sections were incubated in 2 M NaCl, PBS for 10 min followed by treatment with 10% BSA, PBS to block nonspecific binding. Slides were then incubated with 10–30 nM FGF-8 or FGF-10 (Peprotech Inc., Rocky Hill, NJ) together with 10–20 nM FGFR2b-Fc or FGFR2c-Fc (R&D Systems, Minneapolis, MN), respectively, which were fused with the human IgG Fc domain, at 4 °C overnight. After five washes with PBS, the bound FGFR-Fc was detected using a Cy3-conjugated anti-human Fc IgG secondary antibody (Chemicon International Inc., Temecula, CA).

RESULTS

Expression Patterns of HS2ST—HS2ST is highly expressed in the developing limb buds of chick embryos (34). Whole-mount *in situ* hybridization showed that HS2ST transcripts were localized uniformly throughout both wing and leg buds at stage 23 (Fig. 1*A*). In a transverse section of the wing bud region, HS2ST expression was strong in the mesenchyme and weak (but significant) in the overlying ectoderm including the AER (Fig. 1, *B* and *C*). This characteristic expression pattern suggests that HS2ST is deeply involved in limb bud development.

Abnormal Limb Bud Development and Outgrowth by HS2ST RNAi—To investigate the role of 2-*O*-sulfated HS in growth factor signaling in limb bud development, siRNA mixtures were transfected into the LPM of the prospective right forelimb region in stage 13-14 embryos via electroporation. HS2ST esiRNA-injected limbs caused abnormal development 2 days after the operation (Fig. 2, *B–E*), whereas PBS-injected limbs showed less abnormality (Fig. 2*A*). The abnormal limb buds were truncated and reduced in size (Fig. 2, *B–D*) or occasionally indented (Fig. 2*E*). When higher concentrations of esiRNA were injected, severe abnormal phenotypes were observed in the limb buds with higher frequency (Table 1). Green fluorescent protein (GFP) signals derived from coelectroporated pEGFP-N1 were observed around truncated regions of injected limb buds (Fig. 2, *B–E*). The skeletal pattern of mild affected limb at 9 days showed a defective digit and shorter structure compared with the uninjected control left limb (Fig. 2, *H* and *I*). Severely truncated buds showed little outgrowth and a markedly affected cartilage pattern at 9 days (Fig. 2, *D*, *F*, and *G*).

Luciferase esiRNA-injected buds showed a low frequency of abnormalities similar to that in the buffer-injected control (Table 1). For example, 150 ng/μl HS2ST esiRNA-injected buds had a higher frequency of abnormalities (26.5%) than 300 ng/μl luciferase esiRNA-injected buds (13.0%). Although it is known that RNAi techniques sometimes cause off-target effects, it is

TABLE 1
Frequency and severity of truncation of siRNA-injected limbs at stage 22-23

Injection		Severity of truncation[a]				
ng/ml	No.	Total	Mild	Moderate	Severe	Indentation
HS2ST esiRNA						
700	55	27 (49.1%)	12 (14.8%)	5 (18.5%)	4 (44.4%)	6 (22.2%)
450	37	12 (32.4%)	2 (33.3%)	4 (16.7%)	2 (16.7%)	4 (33.3%)
250	62	16 (25.8%)	7 (56.3%)	9 (43.7%)	0 (0%)	0 (0%)
150	78	20 (25.64%)	7 (50.0%)	10 (35.0%)	1 (5.0%)	2 (10.0%)
Luciferase esiRNA						
700	18	4 (22.2%)	3 (25.0%)	1 (75.0%)	0 (0%)	0 (0%)
300	23	3 (13.0%)	2 (33.3%)	1 (66.7%)	0 (0%)	0 (0%)
Buffer (PBS)						
0	84	11 (13.1%)	8 (27.3%)	3 (72.7%)	0 (0%)	0 (0%)

[a] Typical examples are shown in Fig. 2, *B–F*.

unlikely that the truncation is due to such effects. Furthermore the frequency of severe phenotypes in these controls was significantly less than that in HS2ST esiRNA-injected buds (Table 1). These results suggest that the injection of HS2ST esiRNA specifically caused truncation of the limb buds. In addition, HS2ST transcripts were reduced in HS2ST RNAi limb buds compared with untreated buds (Fig. 1, *D–F*). No reduction of HS2ST mRNA was observed in control limb buds (data not shown). These results indicate that siRNA mixtures effectively reduce HS2ST transcripts.

Alteration of HS Structures by HS2ST RNAi—We then examined whether the abnormal morphology of limb buds resulted from the loss of 2-*O*-sulfate residues in HS. Because no suitable antibodies for the detection of 2-*O*-sulfate residues in HS are available, we took advantage of the following binding properties of exogenous FGF-2 to HS to determine the distribution of 2-*O*-sulfated HS in tissues (40). We have shown that 2-*O*-sulfated HS is sufficient to bind FGF-2 (21). We pretreated the limb bud sections with 2 M NaCl to remove endogenous HBGFs, including FGF-2, bound to HS and then stained the sections with exogenous FGF-2 in combination with anti-FGF-2 antibody (Fig. 3 and supplemental Fig. 1). In the normal limb bud at stage 23, exogenous FGF-2 was strongly bound to the basement membranes and mesenchyme underneath the ectoderm (Fig. 3*B* and supplemental Fig. 1). These staining patterns coincided with HS distribution in the limb detected by 3G10 antibody (Fig. 3*A* and supplemental Fig. 1). When sections were treated with heparitinases before applying FGF-2, the FGF-2 binding region was markedly reduced, suggesting that exogenous FGF-2 binds specifically to HS (supplemental Fig. 1). These results indicate that 2-*O*-sulfated HS is abundant in the basement membranes and mesenchyme under the ectoderm in the developing limb bud. We then tested FGF-2 binding activity in siRNA-injected limb buds at stage 23 (Fig. 3). In RNAi-treated limb buds, exogenous FGF-2 bound only weakly to the truncated region compared with the unaffected region, whereas HS distributions themselves were not affected (Fig. 3, *E–H*). We could not see such a decrease of exogenous FGF-2 binding in luciferase RNAi-treated limb buds (data not shown). These results show that HS2ST RNAi also reduced 2-*O*-sulfation and FGF-2 binding. Interestingly 2-*O*-sulfation was significantly reduced in the basement membranes (Fig. 3, *E* and *F*, *arrowheads*). The decrease of 2-*O*-sulfation in the basement membranes could affect the movement of HBGFs between the mesoderm and ectoderm.

Effects on FGF Signaling Loop—To investigate whether HS2ST RNAi disrupted FGF signaling during limb bud development, we examined *Fgf-8* expression using whole-mount *in situ* hybridization of stage 22-23 limb buds (Fig. 4). A marked reduction of *Fgf-8* transcripts was observed in truncated buds by siRNA injection, whereas *Fgf-8* is expressed in the AER of untreated buds (Fig. 4, *A* and *B*). *Shh*, which is induced by FGF-8 signaling, was also reduced in limbs that showed decreased *Fgf-8* expression (Fig. 4*B*, *arrowhead*). In some cases (4 of 13 samples), the reduction of *Fgf-8* expression was also observed even in HS2ST esiRNA-injected but almost normally developed limb buds (Fig. 4*C*); however, no such reduction was observed in luciferase esiRNA-injected limb buds (11 samples).

We also examined Fgf expression in early developmental stages. Chick wing buds develop and grow at stages 18 and 19 at which point *Fgf-8* expression is detectable in the ectoderm (43). In the present study, *Fgf-8* expression was significantly reduced in the ectoderm of RNAi-treated limb buds compared with the untreated opposite limb bud (Fig. 5, *A* and *B*). In a few cases, *Fgf-8* expression was almost undetectable at this stage (Fig. 5*B*, *arrow*). As *Fgf-8* expression is induced by FGF-10 derived from the mesoderm and *Fgf-10* expression is maintained by FGF-8 derived from the AER (5, 6), we examined *Fgf-10* expression in RNAi-treated limb buds at similar stages. Similar to *Fgf-8*, *Fgf-10* expression in the mesoderm was also reduced in siRNA-injected buds (Fig. 5, *C* and *D*). Taken together, these results suggest that a reduction of 2-*O*-sulfated HS down-regulates both *Fgf-8* and *Fgf-10* expression in the developing limb bud.

Up-regulation of ERK and Akt Pathway—The intracellular response to FGFs is mediated by several signal transduction pathways including the MAPK/ERK and phosphatidylinositol 3-OH-kinase/Akt pathways. Recently both pathways have been shown to be essential for limb bud development and patterning (44–46). We examined the activation of ERK and Akt, which are activated in the MAPK and phosphatidylinositol 3-OH-kinase pathways, respectively. We dissected stage 23 esiRNA-injected right limb buds and untreated opposite left limb buds and probed for pERK, ERK, and pAkt by Western blot analysis. The truncated limb buds among those treated with HS2ST esiRNA showed approximately 2 times higher pERK levels than those of the untreated buds, although total ERK levels were not altered between the RNAi-treated and untreated buds (Fig. 6, *A* and *B*, *Group 1*). Similarly pAkt was also increased about 2-fold in the HS2ST RNAi limb buds (Fig. 6, *A* and *B*). No up-regulation of the phosphorylation of ERK and Akt was observed in